

1 **Evaluation of an operational ocean model configuration at**
2 **1/12° spatial resolution for the Indonesian seas**
3 **(NEMO2.3/INDO12) - Part 2: Biogeochemistry**

4
5 **E. Gutknecht¹, G. Reffray¹, M. Gehlen², I. Triyulianti³, D. Berlianty³, and P.**
6 **Gaspar⁴**

7 [1]{Mercator Ocean, 8-10 rue Hermès, 31520 Ramonville, France}

8 [2]{LSCE, UMR CEA-CNRS-UVSQ, Saclay, L'Orme des Merisiers, 91191 Gif-sur-Yvette,
9 France}

10 [3]{Institute for Marine Research and Observation, Jl. Baru Perancak, Negara-Jembrana, Bali
11 82251, Republic of Indonesia}

12 [4]{CLS, 8-10 rue Hermès, 31520 Ramonville, France}

13 Correspondence to: E. Gutknecht (elodie.gutknecht@mercator-ocean.fr)

14
15 **Abstract**

16 In the framework of the INDES0 (Infrastructure Development of Space Oceanography)
17 project, an operational ocean forecasting system was developed to monitor the state of the
18 Indonesian seas in terms of circulation, biogeochemistry and fisheries. This forecasting
19 system combines a suite of numerical models connecting physical and biogeochemical
20 variables to population dynamics of large marine predators (tunas). The
21 physical/biogeochemical coupled component (the INDO12BIO configuration) covers a large
22 region extending from the Western Pacific Ocean to the Eastern Indian Ocean at 1/12°
23 horizontal resolution. The NEMO-OPA physical ocean model and the PISCES
24 biogeochemical model are running simultaneously (“on-line” coupling), at the same
25 resolution. The operational global ocean forecasting system (1/4°) operated by Mercator
26 Ocean provides the physical forcing, while climatological open boundary conditions are
27 prescribed for the biogeochemistry.

1 This paper describes the skill assessment of the INDO12BIO configuration. Model skill is
2 assessed by evaluating a reference hindcast simulation covering the last 8 years (2007-2014).
3 Model results are compared to satellite, climatological and *in-situ* observations. Diagnostics
4 are performed on nutrients, oxygen, chlorophyll-*a*, net primary production, and
5 mesozooplankton.

6 The model reproduces large scale distributions of nutrients, oxygen, chlorophyll-*a*, net
7 primary production and mesozooplankton biomasses. Modelled vertical distributions of
8 nutrients and oxygen are comparable to *in-situ* datasets although gradients are slightly
9 smoothed. The model simulates realistic biogeochemical characteristics of North Pacific
10 tropical waters entering in the archipelago. Hydrodynamics transformation of water masses
11 across the Indonesian archipelago allows conserving nitrate and oxygen vertical distribution
12 close to observations, in the Banda Sea and at the exit of the archipelago. While the model
13 overestimates the mean surface chlorophyll-*a*, the seasonal cycle is in phase with satellite
14 estimations, with higher chlorophyll-*a* concentrations in the southern part of the archipelago
15 during SE monsoon, and in the northern part during NW monsoon. The time-series of
16 chlorophyll-*a* anomalies suggests that meteorological and ocean physical processes that drive
17 the interannual variability of biogeochemical properties in the Indonesian region are
18 reproduced by the model.

19

20 **1 Introduction**

21 The “Coral triangle” delineated by Malaysia, the Philippines, New Guinea, Solomon Islands,
22 East-Timor and Indonesia is recognized as a global hotspot of marine biodiversity (Allen and
23 Werner, 2002; Mora et al., 2003; Green and Mous, 2004; Allen, 2008). It gathers 20% of the
24 world’s species of plants and animals, and the greatest concentration and diversity of reefs
25 (76% of the world’s coral species; Veron et al., 2009). The Indonesian archipelago is located
26 at the centre of this ecologically rich region. It is characterized by a large diversity of coastal
27 habitats such as mangrove forests, coral reefs and sea grass beds, all of which shelter
28 ecosystems of exceptional diversity (Allen and Werner, 2002). The archipelago's natural
29 heritage represents an important source of income and employment, with its future critically
30 depending on the sustainable management of ecosystems and resources (e.g. Foale et al.,
31 2013; Cros et al., 2014).

1 The wider Coral Triangle and its sub-region, the Indonesian archipelago, are facing multiple
2 threats resulting from demographic growth, economic development, change in land use
3 practices and deforestation, as well as global climate change
4 (<http://www.metoffice.gov.uk/media/pdf/8/f/Indonesia.pdf>; FAO, 2007). Human activities
5 cause changes in the delivery of sediments, nutrients and pollutants to coastal waters, leading
6 to eutrophication, ecosystem degradation, as well as species extinctions (Ginsburg, 1994;
7 Pimentel et al., 1995; Bryant et al., 1998; Roberts et al., 2002; UNEP, 2005; Alongi et al.,
8 2013). Surveys report an over 30% reduction of mangroves in Northern Java over the last 150
9 years and an increase of coral reef degradation from 10% to 50% in the last 50 years (Bryant
10 et al., 1998; Hopley and Suharsono, 2000; UNEP, 2009), leading to 80% of the reefs being at
11 risk in this region (Bryant et al., 1998). These changes not only damage coastal habitats, but
12 also propagate across the whole marine ecosystem from nutrients and the first levels of the
13 food web up to higher trophic levels, along with concomitant changes in biogeochemical
14 cycles.

15 There is thus a vital need for monitoring and forecasting marine ecosystem dynamics. The
16 INDESO project (Infrastructure Development of Space Oceanography,
17 www.indeso.web.id/indeso_wp/index.php), funded by the Indonesian Ministry of Marine
18 Affairs and Fisheries, aims at the development of sustainable fishery practices in Indonesia,
19 the monitoring of its Exclusive Economic Zone (EEZ) and the sustainable management of its
20 ecosystems. The project addresses the Indonesian need for building a national capability for
21 operational oceanography. The model system consists of three models deployed at the scale of
22 the Indonesian archipelago: an ocean circulation model (NEMO-OPA; Madec, 2008), a
23 biogeochemical model (PISCES; Aumont and Bopp, 2006) with a spatial resolution of $1/12^\circ$,
24 as well as an intermediate trophic level/fish population dynamics model (SEAPODYM;
25 Lehodey et al., 2008). Since mid-September 2014, the chain of models is fully operational in
26 Perancak (Bali, Indonesia) and delivers 10-day forecast / two weeks hindcast on a weekly
27 basis (see <http://www.indeso.web.id>).

28 The regional ocean dynamics is fully described in Tranchant et al. (this volume, hereafter Part
29 1). The physical model reproduces main processes occurring in this complex oceanic region.
30 Ocean circulation and water mass transformation through the Indonesian Archipelago are
31 close to observations. Eddy Kinetic Energy displays patterns similar to satellite estimates,

1 tides being a dominant forcing in the area. The volume transport of the Indonesian
2 ThroughFlow is comparable to INSTANT data. TS diagrams highlight the erosion of South
3 and North Pacific subtropical waters while crossing the archipelago.

4 The present paper (Part 2) focuses on ocean biogeochemistry. It is organized as follows. The
5 next section presents an overview of the area of study with emphasis on main drivers of
6 biological production over the Indonesian archipelago. The biogeochemical component of the
7 physical-biogeochemical coupled configuration is described in Section 3. Satellite,
8 climatological and *in-situ* observations used to evaluate simulation results are detailed in
9 Section 4. Section 5 presents the evaluation of the skill of the coupled model to reproduce
10 main biogeochemical features of Indonesian seas along with their seasonal and interannual
11 dynamics. Finally, discussion and conclusion are presented in Section 6.

12

13 **2 Area of study**

14 The Indonesian archipelago is crossed by North and South Pacific waters that converge in the
15 Banda Sea, and leave the archipelago through three main straits: Lombok, Ombai and Timor.
16 This ocean current (Indonesian ThroughFlow; ITF) provides the only low-latitude pathway
17 for warm, fresh waters to move from the Pacific to the Indian Ocean (Gordon, 2005; Hirst and
18 Godfrey, 1993). On their way through the Indonesian archipelago, water masses are
19 progressively transformed by surface heat and freshwater fluxes and intense vertical mixing
20 linked to strong internal tides trapped in the semi-enclosed seas as well as upwelling
21 processes (Field and Gordon, 1992). The main flow, as well as the transformation of Pacific
22 waters is correctly reproduced by the physical model, with a realistic distribution of the
23 volume transport through the three major outflow passages (Part 1). In the Indian Ocean, this
24 thermocline water mass forms a cold and fresh tongue between 10°S and 20°S, and supplies
25 the Indian Ocean with nutrients. These nutrients impact biogeochemical cycles and support
26 new primary production in the Indian Ocean (Ayers et al., 2014).

27 Over the archipelago, complex meteorological and oceanographic conditions drive the
28 distribution and growth of phytoplankton and provide favourable conditions for the
29 development of a diverse and productive food web extending from zooplankton, and
30 intermediate trophic levels to pelagic fish (Hendiarti et al., 2004, 2005; Romero et al., 2009).

1 The tropical climate is characterized by a monsoon regime and displays a well-marked
2 seasonality. The south-east (SE) monsoon (April to October) is associated with easterlies
3 from Australia that carry warm and dry air over the region. Wind-induced upwelling along the
4 southern coasts of Sumatra, Java and Nusa-Tenggara Islands (hereafter named Sunda Islands)
5 and in the Banda Sea is associated with high chlorophyll-*a* levels (Susanto et al., 2006; Rixen
6 et al., 2006). Chlorophyll-*a* maxima along Sunda Islands move to the west over the period of
7 the SE monsoon, in response to the alongshore wind shift and associated movement of the
8 upwelling centre (Susanto et al., 2006). From October to April, the north-west (NW) monsoon
9 is associated with warm and moist winds from the Asian continent. Winds blow in a south-
10 west direction north of the Equator and towards Australia south of the Equator. They generate
11 a downwelling and a reduced chlorophyll-*a* content south of the Sunda Islands and in the
12 Banda Sea. The NW monsoon also causes some of the highest precipitation rates in the world.
13 Increased river runoff carries important sediment loads (20 to 25% of the global riverine
14 sediment discharge; Milliman et al., 1999), along with carbon and nutrients to the ocean.
15 These inputs are a strong driver of chlorophyll-*a* variability and play a key role in modulating
16 the biological carbon pump across Indonesian seas (Hendiarti et al., 2004; Rixen et al., 2006).
17 High levels of suspended matter decrease the water transparency in coastal areas and modify
18 the optical properties of waters, which in turn interferes with ocean colour remote sensing
19 (Susanto et al., 2006). Although several Indonesian rivers are classified among the 100 most
20 important rivers of the world, most of them are not regularly monitored. It is thus currently
21 impossible to estimate the impact of river runoff on the variability of chlorophyll-*a* in the
22 region (Susanto et al., 2006).

23 Indonesian seas are also greatly influenced by modes of natural climate variability owing to
24 its position on the equator between Asia and Australia and between the Pacific and Indian
25 Oceans. Strength and timing of the seasonal monsoon are modulated by interannual
26 phenomena that disturb atmospheric conditions and ocean currents. A significant correlation
27 between the variability of the Indonesian ThroughFlow (ITF) and the El Niño-Southern
28 Oscillation (ENSO) was reported (e.g. Meyers, 1996; Murtugudde et al., 1998; Potemra et al.,
29 1997), with ENSO modulating rainfall and chlorophyll-*a* on inter-annual timescales (Susanto
30 et al., 2001, 2006; Susanto and Marra, 2005). ENSO can be monitored using a Multivariate
31 ENSO Index (MEI; Wolter and Timlin, 1993, 1998; <http://www.esrl.noaa.gov/psd/enso/mei/>).

1 In the Eastern Indian Ocean, large anomalies off Sumatra and Java coasts are associated with
2 the Indian Ocean Dipole (IOD) Mode monitored via the Dipole Mode Index (DMI; Saji et al.,
3 1999). A strong positive index points to abnormally strong coastal upwelling and a large
4 phytoplankton bloom near Java Island (Meyers, 1996; Murtugudde et al., 1999). Inside the
5 archipelago, effects of ENSO and IOD climate modes are more difficult to discriminate as
6 they both influence ITF transport. There is, however, evidence for Indian Ocean dynamics to
7 dominate over Pacific Ocean dynamics as drivers of ITF transport variability (Masumoto,
8 2002; Sprintall and Révelard, 2014).

9 Finally, tides, the Madden-Julian Oscillation, Kelvin and Rossby waves are additional drivers
10 of variability across Indonesian seas and influence marine ecosystems (Madden and Julian,
11 1994; Field and Gordon, 1996; Sprintall et al., 2000; Susanto et al., 2000, 2006).

12

13 **3 The INDO12BIO configuration**

14 **3.1 The coupled model**

15 In the framework of the INDESO project, a physical-biogeochemical coupled model is
16 deployed over the domain from 90°E-144°E to 20°S-25°N, widely encompassing the whole
17 Indonesian archipelago, with a spatial resolution of 1/12°. The physical model is based on the
18 NEMO-OPA 2.3 circulation model (Madec et al., 1998; Madec, 2008). Specific
19 improvements include time-splitting and non-linear free surface to correctly simulate high
20 frequency processes such as tides. A parameterization of the vertical mixing induced by
21 internal tides has been developed especially for NEMO-OPA (Koch-Larrouy et al., 2007,
22 2010) and is used here. The physical configuration called INDO12 is described in detail in
23 Part 1.

24 Dynamics of biogeochemical properties across the area are simulated by the PISCES model
25 version 3.2 (Aumont and Bopp, 2006). PISCES simulates the first levels of the marine food
26 web from nutrients up to mesozooplankton. It has 24 state variables. PISCES considers five
27 limiting nutrients for phytoplankton growth (nitrate and ammonium, phosphate, dissolved
28 silica and iron). Four living size-classified compartments are represented: two phytoplankton
29 groups (nanophytoplankton and diatoms) prognostically predicted in carbon (C), iron (Fe),

1 silica (Si) (the latter only for diatoms) and chlorophyll content, and two zooplankton groups
2 (microzooplankton and mesozooplankton). Constant C/N/P Redfield ratios are supposed for
3 all species. While internal Fe/C and Si/C ratios of phytoplankton are modelled as a function of
4 the external availability of nutrients and thus variable, only C is prognostically modelled for
5 zooplankton. The model includes five non-living compartments: small and big particulate
6 organic carbon and semi-labile Dissolved Organic Carbon (DOC), particulate inorganic
7 carbon (CaCO₃ as calcite) and biogenic silica. PISCES also simulates Dissolved Inorganic
8 Carbon (DIC), total alkalinity (carbonate alkalinity + borate + water), and dissolved oxygen.
9 The CO₂ chemistry is computed following the OCMIP protocols
10 (<http://ocmip5.ipsl.jussieu.fr/OCMIP/>). Biogeochemical parameters are based on the standard
11 PISCES namelist version 3.2. Please refer to Aumont and Bopp (2006) for a comprehensive
12 description of the model (version 3.2).

13 PISCES is coupled to NEMO-OPA via the TOP component that manages the
14 advection/diffusion equations of passive tracers and biogeochemical source and sink terms. In
15 our regional configuration, called INDO12BIO, physics and biogeochemistry are running
16 simultaneously (“on-line” coupling), at the same resolution. Particular attention must be paid
17 to respect a number of fundamental numerical constraints. 1/ The numerical scheme of
18 PISCES for biogeochemical processes is forward in time (Euler), which does not correspond
19 to the classical leap-frog scheme used for the physical component. Moreover, the free surface
20 explicitly solved by the time splitting method is non linear. In order to respect the
21 conservation of the tracers, the coupling between biogeochemical and physical components is
22 done every second time step. As a result, the biogeochemical model is controlled by only one
23 leap-frog trajectory of the dynamical model. The use of an Asselin filter allows keeping the
24 two numerical trajectories close enough to overcome this shortcoming. The advantage is a
25 reduction of numerical cost and a time step for the biogeochemical model twice that of the
26 physical component i.e. 900 seconds. 2/ As this time step is small, no time-splitting was used
27 in the sedimentation scheme. 3/ The advection scheme is the standard scheme of TOP-
28 PISCES i.e. the Monotonic Upstream centered Scheme for Conservation Laws (MUSCL)
29 (Van Leer, 1977). No explicit diffusion has been added as the numerical diffusion introduced
30 by this advection scheme is already important.

1 **3.2 Initial and open boundary conditions**

2 The simulation starts on January 3rd, 2007 from the global ocean forecasting system at 1/4°
3 operated by Mercator Ocean (PSY3 described in Lellouche et al., 2013) for temperature,
4 salinity, currents, and free surface at the same date. Open boundary conditions (OBC) are also
5 provided by daily outputs of this system. A 1° thick buffer layer allows nudging the signal at
6 the open boundaries.

7 For biogeochemistry, initial and open boundary conditions are summarized in Table 1.
8 Nitrate, phosphate, dissolved silica, oxygen, DIC, and alkalinity are derived from
9 climatological data sets. For tracers for which this information is missing, initial and open
10 boundary conditions come either from a global scale simulation, are estimated from satellite
11 data, or are build using analytical values. The global scale model NEMO-OPA/PISCES has
12 been integrated for 3000 years at 2° horizontal resolution, until PISCES reached a quasi
13 steady-state (see Aumont and Bopp, 2006). A monthly climatology was built for dissolved
14 iron and DOC based on this simulation. A Dirichlet boundary condition is used to improve the
15 information exchange between the OBC and the interior of the domain.

16 **3.3 External inputs**

17 Three different sources are supplying the ocean in nutrients: atmospheric dust deposition,
18 sediment mobilization, and rivers. Atmospheric deposition of iron comes from the
19 climatological monthly dust deposition simulated by the model of Tegen and Fung (1995),
20 and that of silica follows Moore et al. (2002). Yearly means of river discharges are taken from
21 the Global Erosion Model (GEM) of Ludwig et al. (1996) for DIC, and from the Global News
22 2 climatology (Mayorga et al., 2010) for nutrients. An iron source corresponding to sediment
23 reductive mobilization on continental margins is also considered. For more details on external
24 supply of nutrients, please refer to the supplementary material of Aumont and Bopp (2006). A
25 finer adaptation of each external source of nutrients is prevented by the crucial lack of *in-situ*
26 measurements in the region of interest.

27 In PISCES, external input fluxes are compensated by a loss to the sediments as particulate
28 organic matter, biogenic silica and CaCO₃. These fluxes correspond to matter definitely lost
29 from the ocean system. The compensation of external input fluxes through output at the lower
30 boundary closes the mass balance of the model. While such equilibrium is a valid assumption

1 at the scale of the global ocean, it is not reached at regional scale. For the INDO12BIO
2 configuration, a decrease of the nutrient and carbon loss to the sediment was introduced
3 corresponding to an increase in the water column remineralization by ~4%. This slight
4 enhancement of water column remineralization leads to higher coastal chlorophyll-*a*
5 concentrations (about +1 mg Chl m⁻³) and enables the model to reproduce the chlorophyll-*a*
6 maxima observed along the coasts of Australia and East Sumatra (not shown).

7 **3.4 Simulation length**

8 The simulation starts on January 3rd, 2007 and operates up to present day as the model
9 currently delivers ocean forecasts. For the present paper, we will analyse the simulation up to
10 December 31, 2014. The spin-up length depends on the biogeochemical tracer (Fig. 1). The
11 total carbon inventory computed over the domain (defined as the sum of all solid and
12 dissolved organic and inorganic carbon fractions, yet dominated by the contribution of DIC)
13 equilibrates within several months. To the contrary, DOC, phosphate (PO₄) and iron (Fe) need
14 several years to stabilize (Fig. 1). The annual mean for year 2011 is used for comparison to
15 satellite products (chlorophyll-*a*, net primary production). For comparison to climatologies
16 (zooplankton, nutrients, oxygen) and analysis of the seasonal cycle, we use years 2010 to
17 2014. Interannual variability is assessed over the whole length of simulation except the first
18 year (2008 to 2014).

19

20 **4 Satellite, climatological and *in-situ* data**

21 Model outputs are compared to satellite, climatological, and *in-situ* observations. These
22 observational data are detailed and described in this section.

23 **4.1 INDOMIX cruise**

24 The INDOMIX cruise on-board Marion Dufresne RV (Koch-Larrouy et al., in revision)
25 crossed the Indonesian archipelago between the 09th and 19th of July 2010, and focused on
26 one of the most energetic sections for internal tides from Halmahera Sea to Ombai Strait.
27 Repeated CTD profiles over 24 hours as well as measurements of oxygen and nutrients were
28 obtained for six stations at the entrance of the archipelago (Halmahera Sea), in the Banda Sea
29 and in the Ombai Strait (three of them are used for validation; cf stations on Fig. 4). This data

1 set provides an independent assessment of model skill. To co-localise model and
2 observations, we took the closest simulated point to the coordinates of the station. 2-day
3 model averages were considered as measurements were performed during 2 consecutive days
4 at the stations selected for validation.

5 **4.2 Nutrients and Oxygen**

6 Modelled nutrient and oxygen distributions are compared to climatological fields of World
7 Ocean Atlas 2009 (WOA 2009, 1° spatial resolution) (Garcia et al., 2010a, 2010b),
8 respectively, the CSIRO Atlas of Regional Seas 2009 (CARS 2009, 0.5° spatial resolution)
9 and discreet observations provided by the World Ocean Database 2009 (WOD 2009). Only
10 nitrate, dissolved silica and oxygen distributions are presented hereafter. Nitrate + ammonium
11 and phosphate are linked by a Redfield ratio in PISCES.

12 **4.3 Chlorophyll-*a***

13 The ocean colour signal reflects a combination of chlorophyll-*a* content, suspended matter,
14 coloured dissolved organic matter (CDOM) and bottom reflectance. Singling out the
15 contribution of phytoplankton's chlorophyll-*a* is not straightforward in waters for which the
16 relative optical contribution of the three last components is significant. This is the case over
17 vast areas of the Indonesian archipelago where river discharges and shallow water depths
18 contribute to optical properties (Susanto et al., 2006). The interference with optically
19 absorbing constituents other than chlorophyll-*a* results in large uncertainties in coastal waters
20 (up to 100%, as compared to 30% for open ocean waters) (Moore et al., 2009). Standard
21 algorithms distinguish between open ocean waters / clear waters (Case-1) and coastal waters /
22 turbid waters (Case-2). The area of deployment of the model comprises waters of both
23 categories and the comparison between modelled chlorophyll-*a* and estimates derived from
24 remote sensing can be only qualitative. Two single-mission monthly satellite products are
25 used for model skill evaluation. MODIS-Aqua (EOS mission, NASA) Level-3 Standard
26 Mapped Image product (NASA Reprocessing 2013.1) covers the whole simulated period
27 (2007-2014). It is a product for Case-1 waters, with a 9 km resolution, and is distributed by
28 the ocean colour project (<http://oceancolor.gsfc.nasa.gov/cms/>). The MERIS (ENVISAT,
29 ESA) L3 product (ESA 3rd reprocessing 2011) is also considered. Its spectral characteristics

1 allow the use of an algorithm for Case-2 waters (MERIS C2R Neural Network algorithm;
2 Doerffer and Schiller, 2007). It has a 4 km resolution and is distributed by ACRI-ST
3 (<http://www.acri-st.fr/>), unfortunately the mission ended in April 2012. So MERIS is only
4 used for the evaluation of the annual mean state.

5 **4.4 Net primary production**

6 Net primary production (NPP) is at the base of the food-chain. *In-situ* measurements of NPP
7 are sparse and we rely on products derived from remote sensing for model evaluation. The
8 link between pigment concentration (chlorophyll-*a*) and carbon assimilation reflects the
9 distribution of chlorophyll-*a* concentrations, but also the uncertainty associated to the
10 production algorithm and the ocean colour product. At present, the community uses three
11 production models. The Vertically Generalized Production Model (VGPM) (Behrenfeld and
12 Falkowski, 1997) estimates vertically integrated NPP as a function of chlorophyll, available
13 light, and photosynthetic efficiency. It is currently considered as the Standard algorithm. The
14 two alternative algorithms are an "Eppley" version of the VGPM (distinct temperature-
15 dependent description of photosynthetic efficiencies) and the Carbon-based Production Model
16 (CbPM; Behrenfeld et al. 2005, Westberry et al. 2008). The latter estimates phytoplankton
17 carbon concentration from remote sensing of particulate scattering coefficients. A complete
18 description of the products is available at www.science.oregonstate.edu/ocean.productivity.
19 Henson et al. (2010) point to the uncertainty of the CbPM algorithm, which yields results that
20 are substantially different from the other algorithms. On other hand, Emerson (2014)
21 recommends the CbPM algorithm for providing the best results when tested at three time
22 series sites (BATS, HOTS and OSP stations). Due to the large uncertainty in production
23 models, here we compare the simulated NPP to NPP derived from the three models
24 aforementioned using MODIS ocean colour data.

25 **4.5 Mesozooplankton**

26 MAREDAT, MARine Ecosystem DATA, (Buitenhuis et al., 2013) is a collection of global
27 biomass datasets for major plankton functional types (e.g. diatoms, microzooplankton,
28 mesozooplankton etc.). Mesozooplankton is the only MAREDAT field covering the
29 Indonesian archipelago. The database provides monthly fields at a spatial resolution of 1°.

1 Mesozooplankton data are described in Moriarty and O'Brien (2013). Samples are taken with a
2 single net towed over a fixed depth interval (e.g. 0-50m, 0-100m, 0-150m, 0-200m...) and
3 represent the average population biomass ($\mu\text{g C l}^{-1}$) throughout a depth interval. For this
4 study, only annual mean mesozooplankton biomasses are used. Monthly fields have a too
5 sparse spatial coverage over the Indonesian archipelago and represent different years. It is
6 thus not possible to extract a seasonal cycle.

7

8 **5 INDO12BIO Evaluation**

9 The ability of the INDO12BIO coupled physical-biogeochemical model to reproduce the
10 observed spatial distribution and temporal variability of biogeochemical tracers is assessed for
11 nutrients and oxygen concentrations, chlorophyll-*a*, vertically integrated NPP and
12 mesozooplankton biomass. Model evaluation focuses on annual mean state, mean seasonal
13 cycle and interannual variability. It is completed by a comparison between model outputs and
14 data from the INDOMIX cruise.

15 **5.1 Annual mean state**

16 **5.1.1 Nutrients and Oxygen**

17 Nitrate and oxygen distributions at 100 m depth are presented on Fig. 2 for CARS, WOA and
18 the model. Dissolved silica has the same distribution as nitrate (not shown). The marked
19 meridional gradient, seen in observations of the Pacific and Indian Oceans, is correctly
20 reproduced by the model. Low nitrate and high oxygen concentrations in the subtropical gyres
21 of the North Pacific and South Indian Oceans are due to Ekman-induced downwelling. Higher
22 nitrate and lower oxygen concentrations in the equatorial area are associated with upwelling.
23 Maxima nitrate concentrations associated with minima oxygen concentrations are noticeable
24 in the Bay of Bengal and Adaman Sea (north of Sumatra and west of Myanmar). They reflect
25 discharges by major rivers (Brahmaputra, Ganges and other river systems) and associated
26 increase in oxygen demand. Low nitrate and high oxygen concentrations at 100 m depth in the
27 Sulawesi Sea reflect the signature of Pacific waters entering in the archipelago, a feature
28 correctly reproduced by the model. The signature slowly disappears as waters progressively
29 mix along their pathways across the archipelago. The resulting higher nitrate and lower

1 oxygen levels at 100 m depth in the Banda Sea are reproduced by the model. Higher nitrate
2 and lower oxygen concentrations off the Java-Nusa-Tenggara island chain in data and model
3 outputs reflect seasonal alongshore upwelling.

4 To evaluate the vertical distribution of simulated nutrient and oxygen concentrations over the
5 Indonesian archipelago, vertical profiles of oxygen, nitrate and dissolved silica are compared
6 to climatologies provided by CARS and WOA, as well as to discreet data from WOD (Fig. 3).
7 Vertical profiles are analysed in key areas for the Indonesian ThroughFlow (Koch-Larrouy et
8 al., 2007): (1) one box in the North Pacific Ocean, which is representative of water masses
9 entering the archipelago, (2) one box in the Banda Sea where Pacific waters are mixed to form
10 the ITF, and (3) one box at the exit of the Indonesian archipelago (Timor Strait).
11 Biogeochemical characteristics of tropical Pacific water masses entering the archipelago are
12 correctly reproduced by the model (Fig. 3). The flow across the Indonesian archipelago and
13 the transformation of water masses simulated by the model result in realistic vertical
14 distributions of nutrients and oxygen concentrations in the Banda Sea. The ITF leaves the
15 archipelago and spreads into the Indian Ocean with a biogeochemical content in good
16 agreement with the data available in the area.

17 However, simulated vertical structures are slightly smoothed compared to data (Fig. 3). The
18 vertical gradient of nitrate is too weak over the first 2000m depth of the water column (North
19 Pacific and Timor), and the area of minima oxygen concentrations is eroded (especially in
20 North Pacific box). This bias is even more pronounced on the vertical gradient of dissolved
21 silica (Fig. 3). The smoothing of vertical structures results from the numerical advection
22 scheme MUSCL currently used in PISCES, which is known to be too diffusive (Lévy et al.,
23 2001).

24 **5.1.2 Chlorophyll-*a* and NPP**

25 The simulation reproduces the main characteristics of the large scale distribution of
26 chlorophyll-*a*, a proxy of phytoplankton biomass (Fig. 4). Pacific and Indian subtropical gyres
27 are characterized by low concentrations due to gyre-scale downwelling and hence a deeper
28 nutricline. Highest concentrations are simulated along the coasts driven by riverine nutrient
29 supply, sedimentary processes, as well as upwelling of nutrient-rich deep waters. In
30 comparison to the Case-1 ocean colour product, the model overestimates the chlorophyll-*a*

1 content on oligotrophic gyres and the cross-shore gradient is too weak. As a result, the mean
2 chlorophyll-*a* concentration over the INDO12BIO domain is higher in the simulation (0.53
3 mg Chl m⁻³ with a spatial standard deviation of 0.92 mg Chl m⁻³ over the domain) compared
4 to MODIS (0.3 ± 0.74 mg Chl m⁻³). The bias (as model – observation) is almost positive
5 everywhere, except around the coasts (discussed later) and in the Sulawesi Sea. As mentioned
6 in the preceding section, optical characteristics of waters over the Indonesian archipelago are
7 closer to Case-2 waters (Moore et al., 2009). Simulated chlorophyll-*a* concentrations are
8 indeed closer to those derived with an algorithm for Case-2 waters (MERIS) and its mean
9 value of 0.48 ± 1.4 mg Chl m⁻³.

10 The model reproduces the spatial distribution, as well the rates of NPP over the model domain
11 (Fig. 5). However, as mentioned before, NPP estimates depend on the primary production
12 model (in this case, VGPM, CbPM, and Eppley) and on the ocean colour data used in the
13 production models. For a single ocean colour product (here MODIS), NPP estimates display a
14 large variability (Fig. 5). Mean NPP over the INDO12BIO domain is 34.5 mmol C m⁻² d⁻¹ for
15 VGPM with a standard deviation over the domain of 33.8 mmol C m⁻² d⁻¹, 40.4 ± 22 mmol C
16 m⁻² d⁻¹ for CbPM and 55 ± 52.7 mmol C m⁻² d⁻¹ for Eppley. NPP estimates from VGPM are
17 characterized by low rates in the Pacific (<10 mmol C m⁻² d⁻¹) and a well marked cross-shore
18 gradient. The use of CbPM results in low coastal NPP and almost uniform rates over a major
19 part of the domain and including the open ocean (Fig. 5). The Eppley production model is the
20 most productive one with rates about 15 mmol C m⁻² d⁻¹ in the Pacific and higher than 300
21 mmol C m⁻² d⁻¹ in the coastal zone. The large uncertainty associated with these products
22 precludes a quantitative evaluation of modelled NPP. Like for chlorophyll-*a*, modelled NPP
23 falls within the range of remote sensing derived estimates, with maybe a too weak cross-shore
24 gradient inherited from the chlorophyll-*a* field. The mean NPP over the INDO12BIO domain
25 is, however, overestimated (61 ± 41.8 mmol C m⁻² d⁻¹).

26 **5.1.3 Mesozooplankton**

27 Mesozooplankton links the first level of the marine food web (primary producers) to the mid-
28 and, ultimately, high trophic levels. Modelled mesozooplankton biomass is compared to
29 observations in Fig. 6. While the model reproduces the spatial distribution of
30 mesozooplankton, it overestimates biomass by a factor 2 or 3. This overestimation is likely
31 linked to the above-described overestimation of chlorophyll-*a* and NPP.

1 **5.2 Mean seasonal cycle**

2 The monsoon system drives the seasonal variability of chlorophyll-*a* over the area of study.
3 Northern and southern parts of the archipelago exhibit a distinct seasonal cycle (Fig. 7, 8 and
4 9). In the southern part, the highest chlorophyll-*a* concentrations occur from June to
5 September (Banda Sea and Sunda area in Fig. 8 and 9) due to upwelling of nutrient-rich
6 waters off Sunda Islands and in the Banda Sea triggered by alongshore south-easterly winds
7 during SE monsoon. The decrease in chlorophyll levels during NW monsoon is the
8 consequence of north-westerly winds and associated downwelling in these same areas. In the
9 northern part, high chlorophyll concentrations occur during NW monsoon (South China Sea
10 in Fig. 7) when moist winds from Asia cause intense precipitations. A secondary peak is
11 observed during NW monsoon in the southern part and during SE monsoon in the northern
12 part due to meteorological and oceanographic conditions described above.

13 The annual signal of chlorophyll-*a* in each grid point gives a synoptic view of the effect of the
14 Asia-Australia monsoon system on the Indonesian archipelago. A harmonic analysis is
15 applied on the time series of each grid point to extract the annual signal in model output and
16 remote sensing data (MODIS). The results of the annual harmonic analysis are summarized in
17 Fig. 10 and highlight the month of maximum chlorophyll-*a* and the amplitude of the annual
18 signal. The timing of maximum chlorophyll-*a* presents a north-south distribution in agreement
19 with the satellite observations. The simulation reproduces the chlorophyll-*a* maxima in July in
20 the Banda Sea and off the south coasts of Java-Nusa-Tenggara. Consistent with observations,
21 simulated chlorophyll-*a* maxima move to the west over the period of the SE monsoon, in
22 response to the alongshore wind shift. North of the Nusa-Tenggara Islands, maxima in
23 January-February are due to upwelling associated with alongshore north-westerly winds. In
24 the South China Sea, maxima spread from July-August in the western part (off Mekong
25 River) and gradually shift up to January-February in the eastern part.

26 The temporal correlation between modelled chlorophyll-*a* and estimates derived from remote
27 sensing is 0.55 over the entire INDO12BIO domain, but reaches 0.78 in the South China Sea,
28 0.81 in the Banda Sea and 0.93 in the Indian Ocean (Fig. 7, 8, 9 and 11). These high
29 correlation coefficients are associated with low normalized standard deviations (close to 1) in
30 the Banda Sea and in the Indian Ocean (Fig. 11) and large amplitudes in simulated and
31 observed chlorophyll-*a* (Fig. 10). Normalized standard deviations are higher in the South-East

1 China Sea, Java and Flores Seas, but also in the open ocean due to larger amplitudes in
2 simulated chlorophyll-*a*. The offshore spread of the high amplitude reflects the too weak
3 cross-shore gradient of simulated chlorophyll-*a* (Section 5.1.2), and leads to an increase of the
4 normalized standard deviation with the distance to the coast. For semi-enclosed seas,
5 however, this result has to be taken with caution as clouds cover these regions almost 50-60%
6 of the time period.

7 The model does not succeed in simulating chlorophyll-*a* variability in the Pacific sector (Fig.
8 10 and 11). This area is close to the border of the modelled domain and is influenced by the
9 OBCs derived from the global operational ocean general circulation model. Analysis of the
10 modelled circulation (Part 1) highlights the role of OBCs in maintaining realistic circulation
11 patterns in this area, which is influenced by the equatorial current system. Part 1 points, in
12 particular, to the incorrect positioning of Halmahera and Mindanao eddies in the current
13 model, which contributes to biases in simulated biogeochemical fields.

14 Finally, correlation is low close to the coasts and the temporal variability of the model is
15 lower than that of the satellite product, with normalized standard deviation < 1 (Fig. 11). The
16 model does not take into account seasonal variations in river discharges. Driven by the
17 monsoon system, seasonal input of river runoff is an important driver of chlorophyll-*a*
18 variability at local scale.

19 **5.3 Interannual variability**

20 Figures 7, 8 and 9 present interannual anomalies of surface chlorophyll-*a* concentrations
21 between 2008 and 2014 for model outputs and MODIS ocean colour averaged over three
22 regions: South China Sea, Banda Sea and Sunda area. Simulated fields and satellite-derived
23 chlorophyll-*a* are in good agreement in terms of amplitude and phasing, with temporal
24 correlation coefficients of 0.56 for South China Sea and Banda Sea and 0.88 for Sunda area.
25 The model simulates a realistic temporal variability suggesting that processes regulating the
26 seasonal as well as interannual variability of the Indonesian region are correctly reproduced.
27 While the mean seasonal cycle of chlorophyll-*a* is driven by the strength and timing of the
28 Asian monsoon, anomalies are driven by interannual climate modes, such as El Niño
29 Southern Oscillation (ENSO) and Indian Ocean Dipole (IOD).

1 IOD drives the chlorophyll-*a* interannual variability in the Eastern Tropical Indian Ocean,
2 with a correlation coefficient of 0.74 (Fig. 9). IOD index and anomalies of chlorophyll-*a* from
3 satellite give a similar correlation coefficient of 0.7. A positive phase of IOD indicates
4 negative SST anomaly in the South-Eastern Tropical Indian Ocean associated with zonal wind
5 anomaly along the equator (Meyers, 1996). The abnormally strong coastal upwelling near the
6 Java Island stimulates a large phytoplankton bloom (Murtugudde et al., 1999). In the Banda
7 Sea and in the South China Sea, no clear impact of ENSO or IOD is detected on the first level
8 of the food chain (Fig. 7, 8). Inside the archipelago, both climate modes affect the variability
9 of the ITF transport and it is not straightforward to separate their individual contribution
10 (Masumoto, 2002; Sprintall and Révelard, 2014).

11 While it is established (see references cited in Section 2) that ENSO and IOD climate modes
12 play a key role in the Indonesian region, their impact on the marine ecosystem remains poorly
13 understood. The length of simulation is too short for a rigorous assessment of the role of these
14 drivers and a direct relationship is only evident in the Indian sector. However, interannual
15 anomalies of simulated chlorophyll-*a* compare well to satellite observations, which suggests
16 that interannual meteorological and ocean physical processes are satisfyingly reproduced by
17 the model.

18 **5.4 INDOMIX cruise**

19 Model results are compared to INDOMIX *in-situ* data at three key locations: (1) the eastern
20 entrance of Pacific waters to the archipelago (station 3, Halmahera Sea), (2) the convergence
21 of the western and eastern pathways (station 4, Banda Sea) where intense tidal mixing and
22 upwelling transforms Pacific waters to form the ITF, and (3) one of the main exit portals of
23 the ITF to the Indian Ocean (station 5, Ombai Strait).

24 The vertical profile of temperature compares well to the data in the Halmahera Sea (Fig. 12).
25 Simulated surface waters are too salty and the subsurface salinity maximum is reproduced at
26 the observed depth, albeit underestimated compared to the data. Waters are more oxygenated
27 in the model over the first 400 m. The model-data bias on temperature, salinity and oxygen
28 suggests that Halmahera Sea thermocline waters are not correctly reproduced by the model in
29 July 2010. The model tends to yield too smooth vertical profiles. Vertical profiles of nitrate
30 and phosphate are well reproduced, while dissolved silica concentrations are overestimated

1 below 200 m depth. It should be noted, however, that 2010 was a strong La Niña year with
2 important modifications in zonal winds, rainfall, river discharges and ocean currents. While
3 interannual variability is taken into account in atmospheric forcing and physical open
4 boundary conditions, external nutrient inputs from rivers are constant, and biogeochemical
5 OBCs come from climatologies. However, dissolved silica profiles computed from the
6 monthly WOA2009 climatology are close to simulated distributions (not shown), suggesting
7 non-standard conditions during the time of the INDOMIX cruise.

8 Despite the bias highlighted for Halmahera Sea station, an overall satisfying correspondence
9 between modelled and observed profiles is found at the Banda Sea (Fig. 13) and Ombai Strait
10 stations (Fig. 14). The comparison of modelled profiles and cruise data along the flow path of
11 waters from the Pacific to the Indian Ocean (from Halmahera to Ombai Strait) suggests that
12 either the Halmahera Sea had no major influence for the ITF formation during the time of the
13 cruise, or that vertical mixing and upwelling processes across the archipelago are strong
14 enough to allow the formation of Indonesian water masses despite biases in source water
15 composition. Alternatively, it could reflect the weak impact of ENSO on biogeochemical
16 tracer distributions inside the archipelago compared to its Pacific border and the dominant
17 role of Indian ocean dynamics on the ITF (Sprintall and Révelard, 2014).

18

19 **6 Discussions and conclusions**

20 The INDESO project aims to monitor and forecast marine ecosystem dynamics in Indonesian
21 waters. A suite of numerical models were coupled for setting up a regional configuration
22 (INDO12) adapted to Indonesian seas. A forecasting oceanographic centre is fully operational
23 in Perancak (Bali, Indonesia) since mid-September 2014. Here we assess the skill of the
24 NEMO-OPA hydrodynamical model coupled to the PISCES biogeochemical model
25 (INDO12BIO configuration). A 8-year long hindcast simulation was launched starting in
26 January 2007 and has caught up with real time. In the following paragraphs, the strengths of
27 the simulation are first reviewed and weaknesses are then discussed.

28 The large scale distribution of nutrient, oxygen, chlorophyll-*a*, NPP and mesozooplankton
29 biomass are well reproduced. The vertical distribution of nutrient and oxygen is comparable
30 to *in-situ* based datasets. Biogeochemical characteristics of North Pacific tropical waters

1 entering in the archipelago are set by the open boundaries. The transformation of water
2 masses by hydrodynamics across the Indonesian archipelago is satisfyingly simulated. As a
3 result, nitrate and oxygen vertical distributions match observations in Banda Sea and at the
4 exit of the archipelago. The seasonal cycle of surface chlorophyll-*a* is in phase with satellite
5 estimations. The northern and southern parts of the archipelago present a distinct seasonal
6 cycle, with higher chlorophyll concentrations in the southern part during SE monsoon, and in
7 the northern part of the archipelago during NW monsoon. The interannual variability of
8 surface chlorophyll-*a* correlates with satellite observations in several regions (South China
9 Sea, Banda Sea and Indian part); this suggests that meteorological and ocean physical
10 processes that drive the interannual variability in the Indonesian region are correctly
11 reproduced by the model. The relative contribution of ENSO and IOD interannual climate
12 modes to the interannual variability of chlorophyll-*a* is still an open question, and will be
13 further investigated.

14 However, mean chlorophyll-*a* ($0.53 \text{ mg Chl m}^{-3}$) and NPP ($61 \text{ mmol C m}^{-2} \text{ d}^{-1}$) are
15 systematically overestimated. Around the coasts, the temporal correlation between simulated
16 chlorophyll-*a* and satellite data breaks down. Simulated vertical profiles of nutrient and
17 oxygen are too diffusive as compared to data.

18 In coastal waters, chlorophyll-*a* concentrations are influenced by sedimentary processes (i.e.
19 remineralization of organic carbon and subsequent release of nutrients) and riverine nutrient
20 input. The slight disequilibrium explicitly introduced between the external input of nutrients
21 and carbon and the loss to the sediment is sufficient to enhance chlorophyll-*a* concentrations
22 along the coasts and to make it comparable with observations. The sensitivity of the model to
23 the balancing of carbon and nutrients at the lower boundary of the domain (“sediment burial”)
24 highlights the need for an explicit representation of sedimentary reactions.

25 In order to further improve modelled chlorophyll-*a* variability along the coast, time-variant
26 river nutrient and carbon fluxes is needed. According to Jennerjahn et al. (2004), river
27 discharges from Java can be increased by a factor of ~ 12 during NW monsoon as compared
28 to SE monsoon. Moreover the maximum fresh water transport and the peak of material
29 reaching the sea can be out of phase depending on the origin of discharged material (Hendiarti
30 et al., 2004). The improved representation of river discharge dynamics and associated
31 delivery of fresh water, nutrients and suspended matter in the model is, however, hampered

1 by the availability of data as most of the Indonesian rivers are currently not monitored
2 (Susanto et al., 2006).

3 Systematic misfits between modelled and observed biogeochemical distributions may in part
4 also reflect inherent properties of implemented numerical schemes. Misfits highlighted
5 throughout this work include too much chlorophyll-*a* and NPP on the shelves, with too weak
6 cross-shore gradients between shelf and open waters, together with noticeable smoothing of
7 vertical profiles of nutrients and oxygen. Currently, the MUSCL advection scheme is used for
8 biogeochemical tracers. This scheme is too diffusive and smooths vertical profiles of
9 biogeochemical tracers. As a result, too much nutrients are injected in the surface layer and
10 trigger high levels of chlorophyll-*a* and NPP. Another advection scheme, QUICKEST
11 (Leonard, 1979) with the limiter of Zalezak (1979), already used in NEMO for the advection
12 scheme of the physical model, has been tested for biogeochemical tracers. Switching from
13 MUSCL to QUICKEST-Zalezak accentuates the vertical gradient of nutrients in the water
14 column and attenuates modelled chlorophyll-*a* and NPP. This advection scheme is not
15 diffusive and its use would be coherent with choices adopted for physical tracers. However, it
16 would result in an overestimation of the vertical gradient of nutrients, and the nutricline
17 would be considerably strengthened. Neither tuning of biogeochemical parameters, nor
18 switching the advection scheme for passive tracers fully resolved the model-data misfits.
19 Hence improving the vertical distribution of nutrients and oxygen, as well as chlorophyll-*a*
20 and NPP in the open ocean and their cross-shore gradient first requires improving the model
21 physics.

22 Finally, monthly or yearly climatologies are currently used for initial and open boundary
23 conditions. Biogeochemical tracers are thus decorrelated from model physics. In order to
24 improve the link between modelled physics and biogeochemistry, weekly or monthly
25 averaged output of the global ocean operational system operated by Mercator Ocean
26 (BIOMER) will be used in the future for the 24 tracers of the biogeochemical model PISCES.
27 BIOMER will couple the physical forecasting system PSY3 to PISCES in off-line mode. The
28 biogeochemical and the physical components of INDOBIO12 will thus be initialized and
29 forced coherently, on the base of the PSY3 forecasting system.

30
31

1 **Code and Data Availability**

2 The INDO12 configuration is based on the NEMO 2.3 version developed by the NEMO
3 consortium. All specificities included in the NEMO code version 2.3 are now freely available
4 in the recent version NEMO 3.6 (<http://www.nemo-ocean.eu>). The biogeochemical model
5 PISCES is coupled to hydrodynamic model by the TOP component of the NEMO system.
6 PISCES 3.2 and its external forcing are also available via the NEMO web site. World Ocean
7 Database and World ocean Atlas are available at <https://www.nodc.noaa.gov>. Glodap data are
8 available at <http://cdiac.ornl.gov/oceans/glodap/GlopDV.html>. MODIS and MERIS ocean
9 colour products are respectively available at <http://oceancolor.gsfc.nasa.gov/cms/> and
10 <http://hermes.acri.fr/>, Primary production estimates based on VGPM, Eppley and CbPM
11 algorithms at http://www.science.oregonstate.edu/ocean_productivity/.

12

1 **Acknowledgements**

2 The authors acknowledge financial support through the INDES0 (01/Balitbang
3 KP.3/INDES0/11/2012) and Mercator Vert (LEFE/GMMC) projects. They thank Christian
4 Ethé for its technical advice on NEMO-OPA/PISCES. Ariane Koch-Larrouy provided
5 INDOMIX data. We also thank our colleagues of Mercator Ocean and CLS for their
6 contribution to the model evaluation (Bruno Levier, Clément Bricaud, Julien Paul) and
7 especially Eric Greiner for his useful recommendations and advice on the manuscript.

1 **References**

- 2 Allen, G. R.: Conservation hotspots of biodiversity and endemism for Indo-Pacific coral reef
3 fishes, *Aquatic Conserv: Mar. Freshw. Ecosyst.*, 18: 541–556, doi:10.1002/aqc.880, 2008.
- 4 Allen, G. R., and Werner, T. B.: Coral Reef Fish Assessment in the ‘Coral Triangle’ of
5 Southeastern Asia, *Environmental Biology of Fishes*, 65(2), 209-214,
6 doi:10.1023/A:1020093012502, 2002.
- 7 Alongi, D. A., da Silva, M., Wasson, R. J., and Wirasantosa, S.: Sediment discharge and
8 export of fluvial carbon and nutrients into the Arafura and Timor Seas: A regional synthesis,
9 *Marine Geology*, 343, 146–158, doi:10.1016/j.margeo.2013.07.004, 2013.
- 10 Aumont, O., and Bopp, L.: Globalizing results from ocean in situ iron fertilization studies,
11 *Global Biogeochem. Cycles*, 20, GB2017, doi:10.1029/2005GB002591, 2006.
- 12 Aumont, O., Maier-Reimer, E., Blain, S., and Monfray, P.: An ecosystem model of the global
13 ocean including Fe, Si, P colimitations. *Global Biogeochem. Cycles*, 17(2), 1060,
14 doi:10.1029/2001GB001745, 2003.
- 15 Ayers, J. M., Strutton, P. G., Coles, V. J., Hood, R. R., and Matear, R. J.: Indonesian
16 throughflow nutrient fluxes and their potential impact on Indian Ocean productivity,
17 *Geophys. Res. Lett.*, 41(14), 5060-5067, doi:10.1002/2014GL060593, 2014.
- 18 Behrenfeld, M. J., and Falkowski, P. G.: Photosynthetic rates derived from satellite-based
19 chlorophyll concentration, *Limnol. Oceanogr.*, 42(1), 1-20, 1997.
- 20 Behrenfeld, M. J., Boss, E., Siegel, D. A., and Shea, D. M.: Carbon-based ocean productivity
21 and phytoplankton physiology from space, *Global Biogeochem. Cycles*, 19(1), GB1006,
22 doi:10.1029/2004GB002299, 2005.
- 23 Bryant, D., Burke, L., McManus, J., and Spalding, M.: *Reefs at Risk: A Map-Based Indicator*
24 *of Potential Threats to the World’s Coral Reefs*, World Resources Institute, Washington, DC;
25 International Center for Living Aquatic Resource Management, Manila; and United Nations
26 Environment Programme–World Conservation Monitoring Centre, Cambridge, 1998.
- 27 Buitenhuis, E. T., Vogt, M., Moriarty, R., Bednaršek, N., Doney, S. C., Leblanc, K., Le
28 Quéré, C., Luo, Y.-W., O'Brien, C., O'Brien, T., Peloquin, J., Schiebel, R., and Swan, C.:

1 MAREDAT: towards a world atlas of MARine Ecosystem DATA, *Earth Syst. Sci. Data*, 5,
2 227-239, doi:10.5194/essd-5-227-2013, 2013.

3 Cros, A., Fatan, N. A. White, A., Teoh S. J., Tan, S., Handayani, C., Huang, C., Peterson, N.,
4 Li, R. V., Siry, H. Y., Fitriana, R., Gove, J., Acoba, T., Knight, M., Acosta, R., Andrew, N.,
5 and Beare, D.: The Coral Triangle Atlas: An Integrated Online Spatial Database System for
6 Improving Coral Reef Management, *PLoS ONE* 9(6): e96332.
7 doi:10.1371/journal.pone.0096332, 2014.

8 CSIRO: Atlas of Regional Seas, available at: <http://www.marine.csiro.au/~dunn/cars2009/>
9 (last access: 13 August 2015), 2009.

10 Doerffer, R. and Schiller, H: The MERIS Case 2 water algorithm, *International Journal of*
11 *Remote Sensing*, 28, 517-535, doi:10.1080/01431160600821127, 2007.

12 FAO: United Nations Food and Agricultural Organization, FAOSTAT, available at:
13 <http://faostat.fao.org/site/291/default.aspx> (last access: 13 August 2015), 2007.

14 Ffield, A., and Gordon, A. L.: Vertical Mixing in the Indonesian Thermocline, *J. Phys.*
15 *Oceanogr.*, 22, 184-195, 1992.

16 Ffield, A., and Gordon, A. L.: Tidal mixing signatures in the Indonesian Seas. *J. Phys.*
17 *Oceanogr.*, 26, 1924–1937, 1996.

18 Foale, S., Adhuri, D., Aliño, P., Allison, E. H., Andrew, N., Cohen, P., Evans, L., Fabinyi,
19 M., Fidelman, P., Gregory, C., Stacey, N., Tanzer, J., and Weeratunge, N.: Food security and
20 the Coral Triangle Initiative, *Marine Policy*, 38, 174-183, doi:10.1016/j.marpol.2012.05.033,
21 2013.

22 Garcia, H. E., Locarnini, R. A., Boyer, T. P., Antonov, J. I., Baranova, O. K., Zweng, M. M.,
23 and Johnson, D. R.: World Ocean Atlas 2009, Volume 3: Dissolved Oxygen, Apparent
24 Oxygen Utilization, and Oxygen Saturation. S. Levitus, Ed. NOAA Atlas NESDIS 70, U.S.
25 Government Printing Office, Washington, D.C., 344 pp., 2010a.

26 Garcia, H. E., Locarnini, R. A., Boyer, T. P., Antonov, J. I., Zweng, M. M., Baranova, O. K.,
27 and Johnson, D. R.: World Ocean Atlas 2009, Volume 4: Nutrients (phosphate, nitrate,
28 silicate). S. Levitus, Ed. NOAA Atlas NESDIS 71, U.S. Government Printing Office,
29 Washington, D.C., 398 pp., 2010b.

- 1 Ginsburg, R. N.: Ed., Proceedings of the Colloquium on Global Aspects of Coral Reefs:
2 Health, Hazards and History, Atlantic Reef Committee, 1994.
- 3 Gordon, A. L: Oceanography of the Indonesian seas and their throughflow, *Oceanography*,
4 18(4), 14–27, doi:10.5670/oceanog.2005.01, 2005.
- 5 Green, A., and Mous, P. J.: Delineating the Coral Triangle, its ecoregions and functional
6 seascapes. Report on an expert workshop held in Southeast Asia Center for Marine Protected
7 Areas, Bali, Indonesia, April 30-May 2, 2003, The Nature Conservancy, 2004.
- 8 Hendiarti, N., Siegel, H., and Ohde, T.: Investigation of different coastal processes in
9 Indonesian waters using SeaWiFS data, *Deep-Sea Research Part II*, 51(1-3), 85-97,
10 doi:10.1016/j.dsr2.2003.10.003, 2004.
- 11 Hendiarti, N., Suwarso, E., Aldrian, E., Amri, K., Andiastuti, R., Sachoemar, S. I., and
12 Wahyono, I. B.: Seasonal variation of pelagic fish catch around Java, *Oceanography*, 18(4),
13 112-123, doi:10.5670/oceanog.2005.12, 2005.
- 14 Henson, S. A., Sarmiento, J. L., Dunne, J. P., Bopp, L., Lima, I., Doney, S. C., John, J., and
15 Beaulieu, C.: Detection of anthropogenic climate change in satellite records of ocean
16 chlorophyll and productivity, *Biogeosciences*, 7(2), 621–640, doi:10.5194/bg-7-621-2010,
17 2010.
- 18 Hirst, A. C., and Godfrey, J. S.: The role of Indonesian ThroughFlow in a global ocean GCM,
19 *J. Phys. Oceanogr.*, 23(6), 1057–1086, 1993.
- 20 Hopley, D. and Suharsono, M.: *The Status of Coral Reefs in Eastern Indonesia*. Australian
21 Institute of Marine Science, Townsville, Australia, 2000.
- 22 Jennerjahn, T. C., Ittekkot, V., Klopper, S., Adi, S., Purwo Nugroho, S., Sudiana, N., Yusmal,
23 A., and Gaye-Haake, B.: Biogeochemistry of a tropical river affected by human activities in
24 its catchment: Brantas River estuary and coastal waters of Madura Strait, Java, Indonesia,
25 *Estuarine Coastal Shelf Sci.*, 60(3), 503–514, doi:10.1016/j.ecss.2004.02.008, 2004.
- 26 Key, R. M., Kozyr, A., Sabine, C. L., Lee, K., Wanninkhof, R., Bullister, J., Feely, R.A.,
27 Millero, F., Mordy, C. and Peng, T.-H.: A global ocean carbon climatology: Results from
28 GLODAP. *Global Biogeochemical Cycles*, Vol. 18, GB4031, 2004.

- 1 Koch-Larrouy, A., Madec, G., Bouruet-Aubertot, P., Gerkema, T., Bessieres, L., and
2 Molcard, R.: On the transformation of Pacific Water into Indonesian Throughflow Water by
3 internal tidal mixing, *Geophys. Res. Lett.*, 34, L04604, doi:10.1029/2006GL028405, 2007.
- 4 Koch-Larrouy, A., Morrow, R., Penduff, T., and Juza, M.: Origin and mechanism of
5 Subantarctic Mode Water formation and transformation in the Southern Indian Ocean, *Ocean
6 Dynamics*, 60(3), 563-583, doi:10.1007/s10236-010-0276-4, 2010.
- 7 Koch-Larrouy, A., Atmadipoera, A., Van Beek, P., Madec, G., Aucan, J., Lyard, F., Grelet, J.
8 and Souhaut, M.: Estimates of tidal mixing in the Indonesian archipelago from
9 multidisciplinary INDOMIX in-situ data, *Deep Sea Research part 1*, M DSR1-D-14-00245R1,
10 in revision, 2015.
- 11 Lehodey, P., Senina, I., and Murtugudde, R.: A spatial ecosystem and populations dynamics
12 model (SEAPODYM) – Modeling of tuna and tuna-like populations, *Progress in
13 Oceanography*, 78, 304–318, 2008.
- 14 Leonard, B. P.: A stable and accurate convective modelling procedure based on quadratic
15 upstream interpolation, *Comp. Method. Appl. M.* 19, 59–98, 1979.
- 16 Lévy, M., Estublier, A., and Madec, G.: Choice of an Advection Scheme for Biogeochemical
17 Models, *Geophysical Research Letters*, 28(19), 3725-3728, 2001.
- 18 Ludwig, W., Probst, J. L., and Kempe, S.: Predicting the oceanic input of organic carbon by
19 continental erosion, *Global Biogeochem.Cycles*, 10(1), 23– 41, doi:10.1029/95GB02925,
20 1996.
- 21 Madden, R. A., and Julian P. R.: Observations of the 40–50 day tropical oscillation - A
22 review, *Monthly Weather Reviews*, 122(5), 814–837, 1994.
- 23 Madec G.: "NEMO ocean engine", Note du Pole de modélisation, Institut Pierre-Simon
24 Laplace (IPSL), France, No 27 ISSN No 1288-1619, 2008.
- 25 Madec, G., Delecluse, P., Imbard, M., and Lévy, C.: "OPA 8.1 Ocean General Circulation
26 Model reference manual", Note du Pole de modélisation, Institut Pierre-Simon Laplace
27 (IPSL), France, No11, 91pp., 1998.
- 28 Masumoto, Y.: Effects of Interannual Variability in the Eastern Indian Ocean on the
29 Indonesian Throughflow, *Journal of Oceanography*, 58, 175-182, 2002.

- 1 Meyers, G.: Variation of Indonesian throughflow and the El Niño-Southern Oscillation. *J.*
2 *Geophys. Res.*, 101, 12,475–12,482, 1996.
- 3 Milliman, J. D., Farnsworth, K. L., and Albertin, C. S.: Flux and fate of fluvial sediments
4 leaving large islands in the East Indies, *J. Sea Res.*, 41(1-2), 97–107, 1999.
- 5 Moore, T. S., Campbell, J. W., and Dowell, M. D: A class-based approach to characterizing
6 and mapping the uncertainty of the MODIS ocean chlorophyll product, *Remote Sensing of*
7 *Environment*, 113, 2424-2430, 2009.
- 8 Mora, C., Chittaro, P. M., Sale, P. F., Kritzer, J. P., and Ludsin, S.A.: Patterns and processes
9 in reef fish diversity, *Nature*, 421, 933-936, doi:10.1038/nature01393, 2003.
- 10 Moriarty, R., and O'Brien, T. D.: Distribution of mesozooplankton biomass in the global
11 ocean, *Earth System Science Data*, 5,45-55, 2013.
- 12 Murtugudde, R., Busalacchi, A. J., and Beauchamp, J.: Seasonal-to-interannual effects of the
13 Indonesian Throughflow on the tropical Indo-Pacific Basin. *J. Geophys. Res.*, 103, 21,425–
14 21,441, 1998.
- 15 Murtugudde, R., Signorini, S. R., Christian, J. R., Busalacchi, A. J., McClain, C. R., and
16 Picaut, J.: Ocean color variability of the tropical Indo-Pacific basin observed by SeaWiFS
17 during 1997–1998. *J. Geophys. Res.*, 104, 18,351–18,366, 1999.
- 18 Pimentel D., Harvey, C., Resosudarmo, P., Sinclair, K., Kurz, D., McNair, M., Crist, C.,
19 Shpritz, L., Fitton, L., Saffouri, R., and Blair, R.: Environmental and Economic Costs of Soil
20 Erosion and Conservation Benefits, *Science*, 267(5201), 1117-1123, 1995.
- 21 Potemra, J. T., Lukas, R., and Mitchum, G. T.: Large-scale estimation of transport from the
22 Pacific to the Indian Ocean. *J. Geophys. Res.*, 102, 27,795–27,812, 1997.
- 23 Rixen, T., Ittekkot, V., Herunadi, B., Wetzel, P., Maier-Reimer, E., and Gaye-Haake, B.:
24 ENSO-driven carbon sea saw in the Indo-Pacific, *Geophys. Res. Lett.*, 33, L07606,
25 doi:10.1029/2005GL024965, 2006.
- 26 Roberts, C. M., McClean, C. J., Veron, J. E. N., Hawkins, J. P., Allen, G. R., McAllister, D.
27 E., Mittermeier, C. G., Schueler, F. W., Spalding, M., Wells, F., Vynne, C., and Werner, T.
28 B.: Marine Biodiversity Hotspots and Conservation Priorities for Tropical Reefs, *Science*,
29 295(5558), 1280-1284, doi10.1126/science.1067728, 2002.

- 1 Romero, O. E., Rixen, T., and Herunadi, B.: Effects of hydrographic and climatic forcing on
2 diatom production and export in the tropical southeastern Indian Ocean, *Mar. Ecol. Prog. Ser.*,
3 384, 69-82, doi:10.3354/meps08013, 2009.
- 4 Saji, N. H., Goswami, B. N., Vinayachandran, P. N., and Yamagata, T.: A dipole mode in the
5 tropical Indian Ocean. *Nature*, 401, 360–363, 1999.
- 6 Sprintall, J., Gordon, A. L., Murtugudde, R., and Susanto, R. D.: A semi-annual Indian Ocean
7 forced Kelvin waves observed in the Indonesian Seas, May 1997. *J. Geophys. Res.*, 105(C7),
8 17217–17230, doi:10.1029/2000JC900065, 2000.
- 9 Sprintall, J., and Révelard, A: The Indonesian throughflow response to Indo-Pacific climate
10 variability, *J. Geophys. Res. Oceans*, 119, 1161–1175, doi:10.1002/2013JC009533, 2014.
- 11 Susanto, R. D., and Marra, J.: Effect of the 1997/98 El Niño on chlorophyll a variability along
12 the southern coasts of Java and Sumatra, *Oceanography*, 18(4), 124–127,
13 doi:10.5670/oceanog.2005.13, 2005.
- 14 Susanto, R. D., Gordon, A. L., Sprintall, J., and Herunadi, B.: Intraseasonal variability and
15 tides in Makassar Strait. *Geophys. Res. Lett.*, 27, 1499–1502, 2000.
- 16 Susanto, R. D., Gordon, A. L., and Zheng, Q.: Upwelling along the coasts of Java and
17 Sumatra and its relation to ENSO, *Geophys. Res. Lett.*, 28(8), 1599-1602,
18 doi:10.1029/2000GL011844, 2001.
- 19 Susanto, R. D., Moore, T. S., and Marra, J.: Ocean color variability in the Indonesian Seas
20 during the SeaWiFS era, *Geochemistry Geophysics Geosystems*, 7(5), Q05021,
21 doi:10.1029/2005GC001009, 2006.
- 22 Tegen, I., and Fung, I.: Contribution to the Atmospheric Mineral Aerosol Load From Land-
23 Surface Modification, *J Geophys Res-Atmos*, 100, 18707–18726, 1995.
- 24 Tranchant, B., Reffray, G., Greiner, E., Nugroho, D., Koch-Larrouy, A., and Gaspar, P.:
25 Evaluation of an operational ocean model configuration at 1/12° spatial resolution for the
26 Indonesian seas (NEMO2.3/INDO12) – Part 1: Ocean physics, *Geosci. Model Dev.*, 9, 1037-
27 1064, doi:10.5194/gmd-9-1037-2016, 2016.
- 28 UNEP: Vantier, L., Wilkinson, C., Lawrence, D. and Souter, D. (Eds.): Indonesian Seas,
29 GIWA Regional Assessment 57, University of Kalmar, Kalmar, Sweden, 2005.

1 UNEP: Sherman, K. and Hempel, G. (Eds.): The UNEP Large Marine Ecosystem Report: A
2 perspective on changing conditions in LMEs of the world's Regional Seas, United Nations
3 Environment Programme. Nairobi, Kenya, 2009.

4 Van Leer, B.: Towards the Ultimate Conservative Difference Scheme. IV. A New Approach
5 to Numerical Convection, *J. Comput. Phys.*, 23, 276-299, 1977.

6 Veron, J. E. E., Devantier, L. M., Turak, E., Green, A. L., Kininmonth, S., Stafford-Smith,
7 M., and Peterson, N.: Delineating the Coral Triangle, *Galaxea, J. Coral Reef Studies* 11, 91-
8 100, 2009.

9 Westberry, T., Behrenfeld, M. J., Siegel, D. A., and Boss, E.: Carbon-based primary
10 productivity modeling with vertically resolved photoacclimation, *Global Biogeochem.*
11 *Cycles*, 22(2), GB2024, doi:10.1029/2007GB003078, 2008.

12 WOA: World Ocean Atlas, available at: http://www.nodc.noaa.gov/OC5/WOA09/pr_
13 [woa09.html](http://www.nodc.noaa.gov/OC5/WOA09/pr_) (last access: 13 August 2015), 2009.

14 WOD: World Ocean Database, available at: http://www.nodc.noaa.gov/OC5/WOD09/pr_
15 [wod09.html](http://www.nodc.noaa.gov/OC5/WOD09/pr_) (last access: 13 August 2015), 2009.

16 Wolter, K., and Timlin, M. S.: Measuring the strength of ENSO events - how does 1997/98
17 rank? *Weather*, 53, 315-324, 1998.

18 Wolter, K., and Timlin, M. S.: El Niño/Southern Oscillation behaviour since 1871 as
19 diagnosed in an extended multivariate ENSO index (MEI.ext). *Intl. J. Climatology*, 31, 1074-
20 1087, 2011.

21 Zalezak, S. T.: Fully multidimensional flux-corrected transport algorithms for fluids, *J.*
22 *Computat. Phys.*, 31, 335-362, 1979.

23

1 **Table caption**

2 Table 1. Initial and open boundary conditions used for the INDO12BIO configuration.

3

4

5 **Figure caption**

6 Figure 1. Temporal evolution of total carbon (a), plankton (b), DIC and DOC (c) and nutrient
7 (d, e) content averaged over the whole 3-dimensional INDO12BIO domain.

8 Figure 2: Annual mean of nitrate (mmol N m^{-3} ; left) and oxygen concentrations ($\text{ml O}_2 \text{ l}^{-1}$;
9 right) at 100 m depth from CARS (a, d) and WOA (b, e; statistical mean) annual
10 climatologies, and from INDO12BIO as 2010-2014 averages (c, f). Three key boxes for water
11 mass transformation (North Pacific, Banda, and Timor; Koch-Larrouy et al., 2007) were
12 added to the bottom-right figure.

13 Figure 3: Vertical profiles of oxygen ($\text{ml O}_2 \text{ l}^{-1}$; top: a, d, g), nitrate (mmol N m^{-3} ; middle: b,
14 e, h) and dissolved silica (mmol Si m^{-3} ; bottom: c, f, i) in 3 key boxes for water masses
15 transformation (North Pacific, left; Banda, middle; and Timor, right) (see Fig. 2; Koch-
16 Larrouy et al., 2007). CARS and WOA annual climatologies are in red and dark blue.
17 INDO12BIO simulation averaged between 2010 and 2014 is in black. All the raw data
18 available on each box and gathered in the WOD (light blue crosses) are added in order to
19 illustrate the spread of data.

20 Figure 4. Left) Annual mean of surface chlorophyll-*a* concentrations (mg Chl m^{-3}) for year
21 2011: MODIS Case-1 product (a), MERIS Case-2 product (b) and INDO12BIO simulation
22 (c). Right) Bias of log-transformed surface chlorophyll (model-observation) for the same
23 year. The model was masked as a function of the observation, MODIS Case-1 (d) or MERIS
24 Case-2 (e). Location of 3 stations sampled during the INDOMIX cruise and used for
25 evaluation of the model in Section 4.4 (f).

26 Figure 5. Annual mean of vertically integrated NPP ($\text{mmol C m}^{-2} \text{ d}^{-1}$) for year 2011: VGPM
27 (a), Eppley (d), and CbPM (b) production models, all based on MODIS ocean colour, as well
28 as for INDO12BIO (e). Standard deviation of the 3 averaged production models (PM) (c), and
29 bias between INDO12BIO and the average of PM (f).

1 Figure 6: Annual mean of mesozooplankton biomass ($\mu\text{g C l}^{-1}$) from MAREDAT monthly
2 climatology (left) and from INDO12BIO simulation averaged between 2010 and 2014 (right),
3 for distinct depth interval: from the surface up to 40m (a, e), 100m (b, f), 150m (c, g), and
4 200m depth (d, h). Simulated fields were interpolated onto the MAREDAT grid, and masked
5 as a function of the data (in space and time).

6 Figure 7: a) Mean surface chlorophyll-*a* concentrations and b) its interannual anomalies (mg
7 Chl m^{-3}) over the South China Sea. INDO12BIO is in black and MODIS Case-1 in red.
8 Temporal correlation (*r*) between both time series is in black. c) ENSO (blue) and IOD
9 (green) phenomena are respectively represented by MEI and DMI indexes. Indexes were
10 normalized by their maximum value in order to be plotted on the same axis. Interannual
11 anomalies of simulated chlorophyll-*a* are reminded in black. Temporal correlation (*r*) between
12 the simulated chlorophyll-*a* and ENSO (IOD) is indicated in blue (green).

13 Figure 8: Same as Figure 7, in Banda Sea.

14 Figure 9: Same as Figure 7, in Sunda area.

15 Figure 10. Timing of maximum chlorophyll-*a* (a, c) and amplitude (b, d) for a monthly
16 climatology of surface chlorophyll-*a* concentrations between 2010 and 2014: MODIS Case-1
17 (left) and INDO12BIO (right). The model was masked as a function of the data.

18 Figure 11: Temporal correlation (a) and normalised standard deviation (b;
19 $\text{std}(\text{model})/\text{std}(\text{data})$) estimated between the INDO12BIO simulation and the MODIS Case-1
20 ocean colour product. Statistics are computed on monthly fields between 2010 and 2014. The
21 model was masked as a function of the data.

22 Figure 12: Vertical profiles of temperature ($^{\circ}\text{C}$; a), salinity (psu; b), oxygen ($\text{ml O}_2 \text{l}^{-1}$; c),
23 nitrate (mmol N m^{-3} ; d), phosphate (mmol P m^{-3} ; e), and dissolved silica (mmol Si m^{-3} ; f)
24 concentrations at INDOMIX cruise Station 3 (Halmahera Sea; 13 - 14 July 2010). CTD (light
25 blue lines) and bottle (red crosses) measurements represent the conditions during cruise, 2-
26 day model averages are shown by the black line.

27 Figure 13: Vertical profiles of temperature ($^{\circ}\text{C}$; a), salinity (psu; b), oxygen ($\text{ml O}_2 \text{l}^{-1}$; c),
28 nitrate (mmol N m^{-3} ; d), phosphate (mmol P m^{-3} ; e), and dissolved silica (mmol Si m^{-3} ; f)
29 concentrations at INDOMIX cruise Station 4 (Banda Sea; 15 - 16 July 2010). CTD (light blue

1 lines) and bottle (red crosses) measurements represent the conditions during cruise, 2-day
2 model averages are shown by the black line.

3 Figure 14: Vertical profiles of temperature ($^{\circ}\text{C}$; a), salinity (psu; b), oxygen ($\text{ml O}_2 \text{ l}^{-1}$; c),
4 nitrate (mmol N m^{-3} ; d), phosphate (mmol P m^{-3} ; e), and dissolved silica (mmol Si m^{-3} ; f)
5 concentrations at INDOMIX cruise Station 5 (Ombai Strait; 16 - 17 July 2010). CTD (light
6 blue lines) and bottle (red crosses) measurements represent the conditions during cruise, 2-
7 day model averages are shown by the black line.

8

1 Table 1. Initial and open boundary conditions used for the INDO12BIO configuration.

2

Variables	Initial Conditions	OBC
NO₃, O₂, PO₄, Si	From WOA January ^a	WOA monthly ^a
DIC, ALK	GLODAP annual ^b	GLODAP annual ^b
DCHL, NCHL, PHY2, PHY1	From SeaWiFS January ^c	From SeaWiFS monthly ^c
NH₄	Analytical profile ^d	Analytical profile ^d
DOC, Fe	ORCA2 January	ORCA2 monthly

3 ^a: From World Ocean Atlas (WOA 2009) monthly climatology, with increased nutrient
4 concentrations along the coasts (necessary adaptation due to crucial lack of data in the studied
5 area).

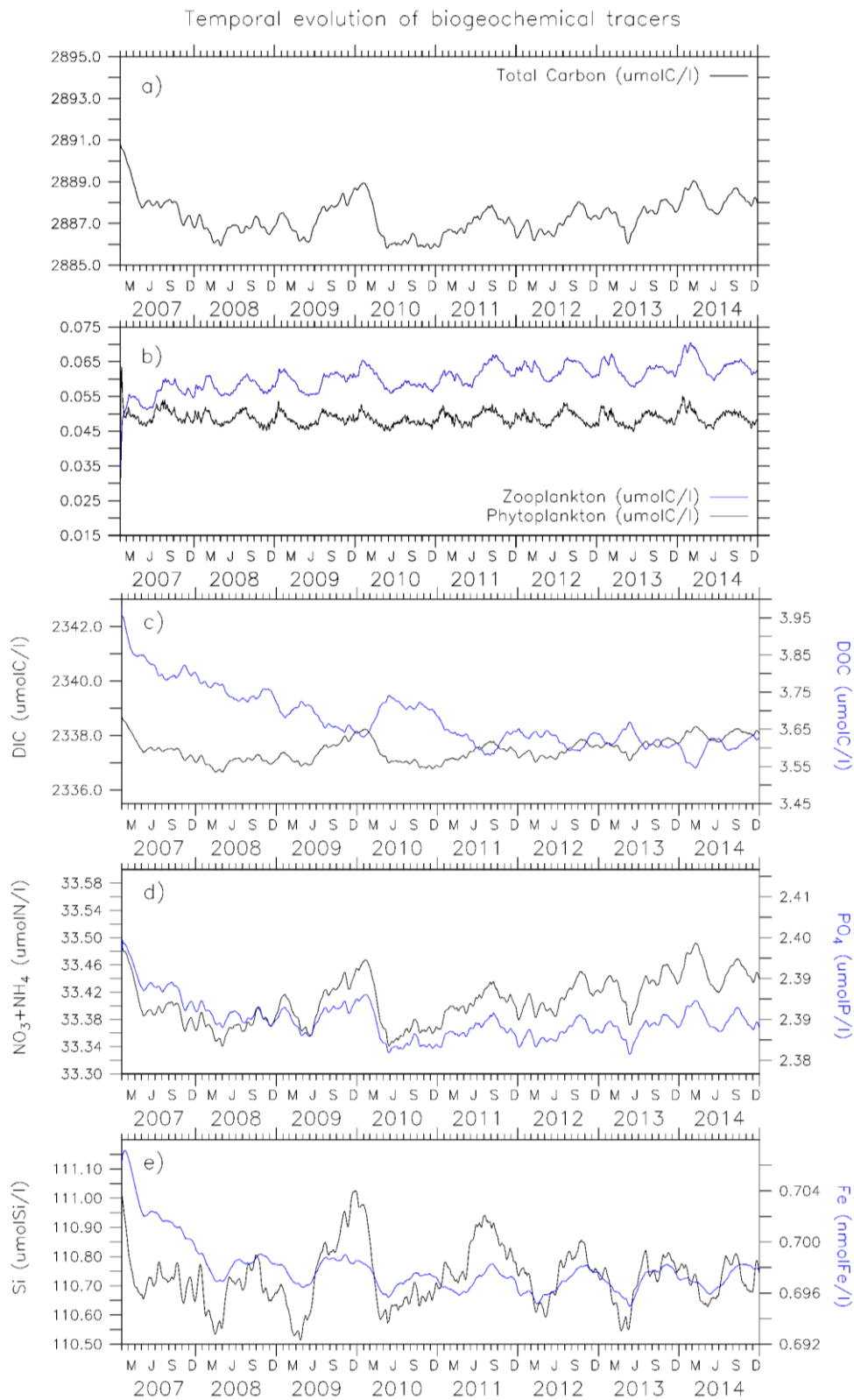
6 ^b: Key et al. (2004).

7 ^c: From SeaWiFS monthly climatology. Phytoplankton is deduced using constant ratios of
8 1.59 g Chl mol N⁻¹ and 122/16 mol C mol N⁻¹, and exponential decrease with depth.

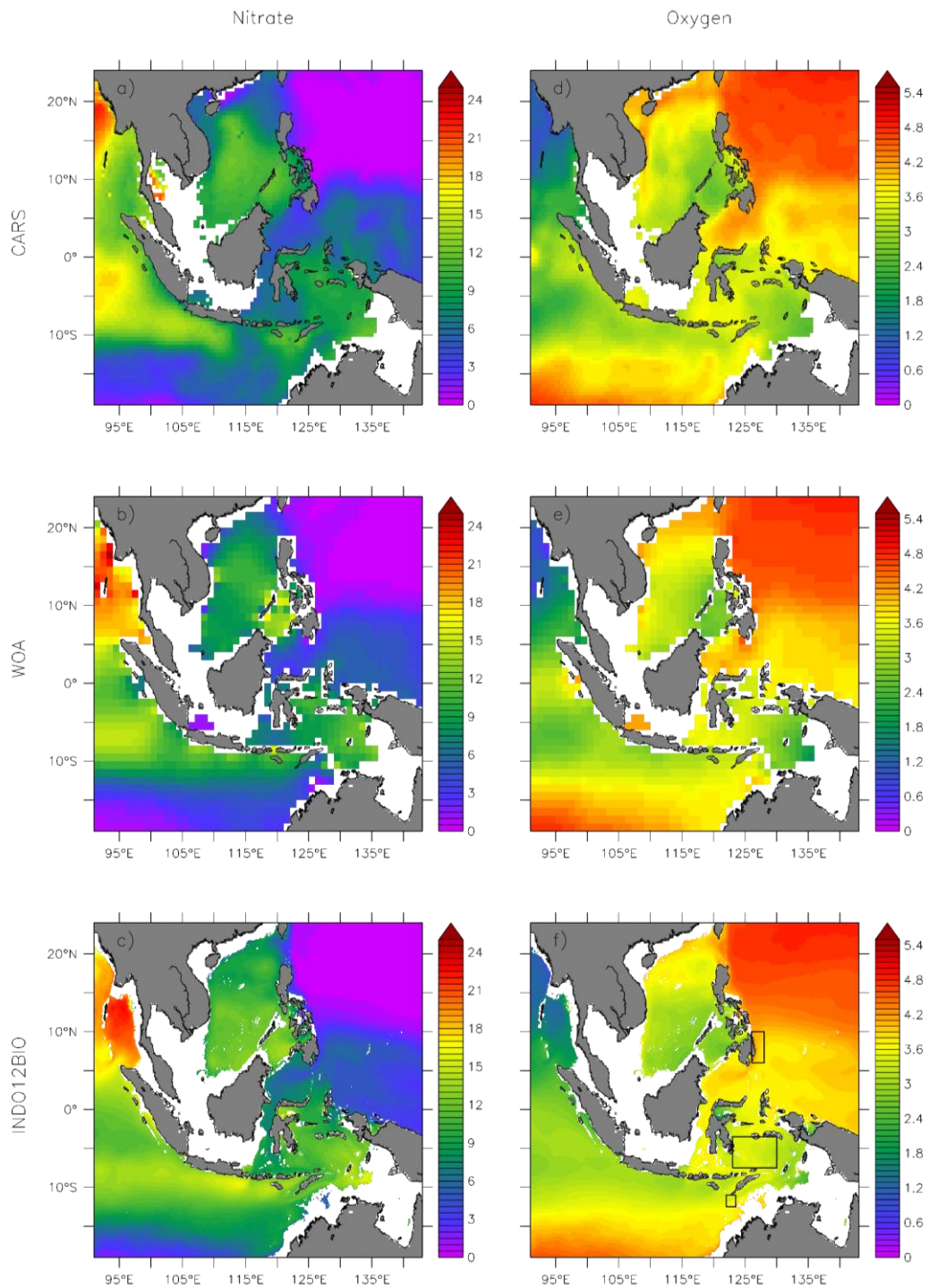
9 ^d: Low values offshore and increasing concentrations onshore.

10

11

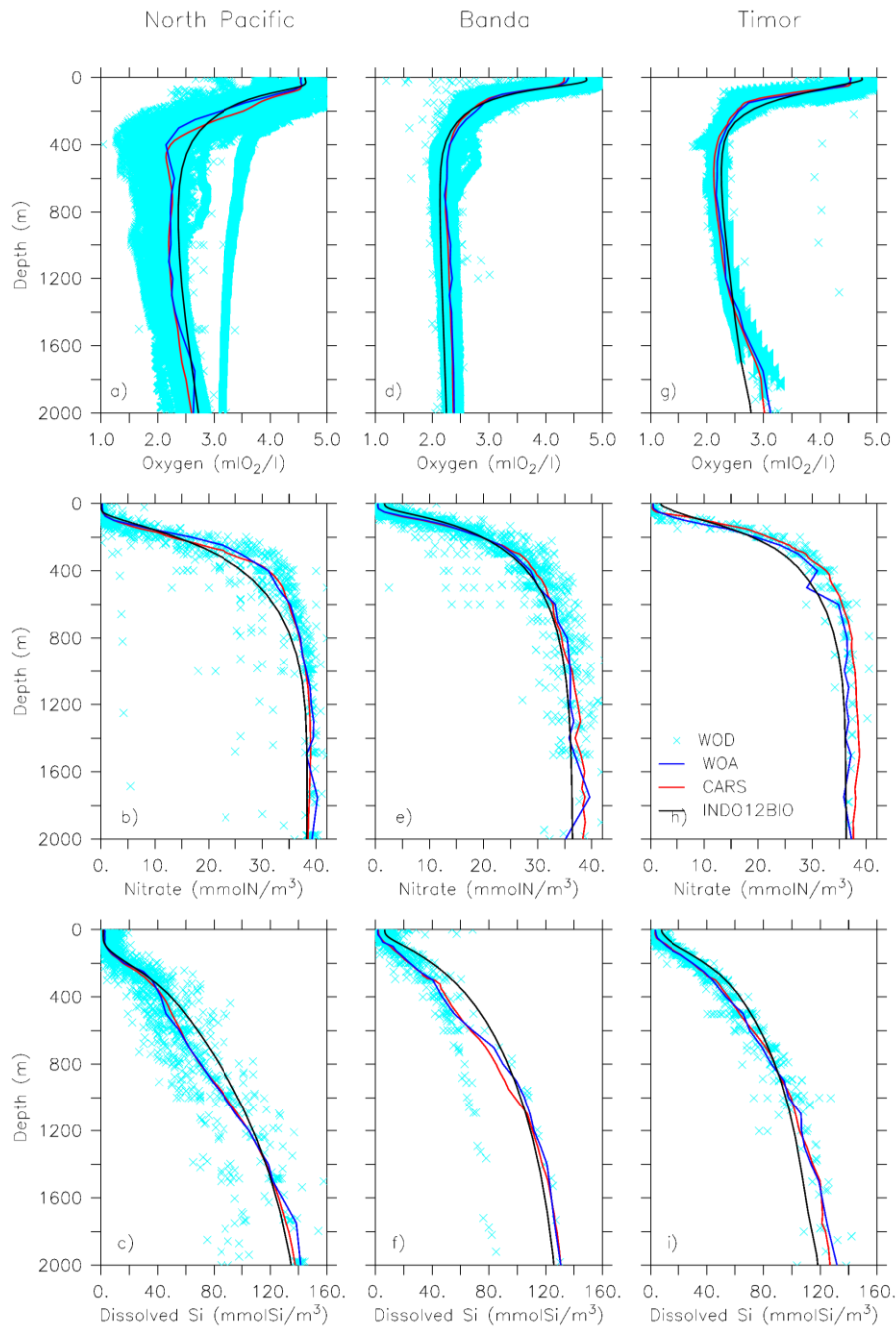


1
 2 Figure 1. Temporal evolution of total carbon (a), plankton (b), DIC and DOC (c) and nutrient
 3 (d, e) content averaged over the whole 3-dimensional INDO12BIO domain.

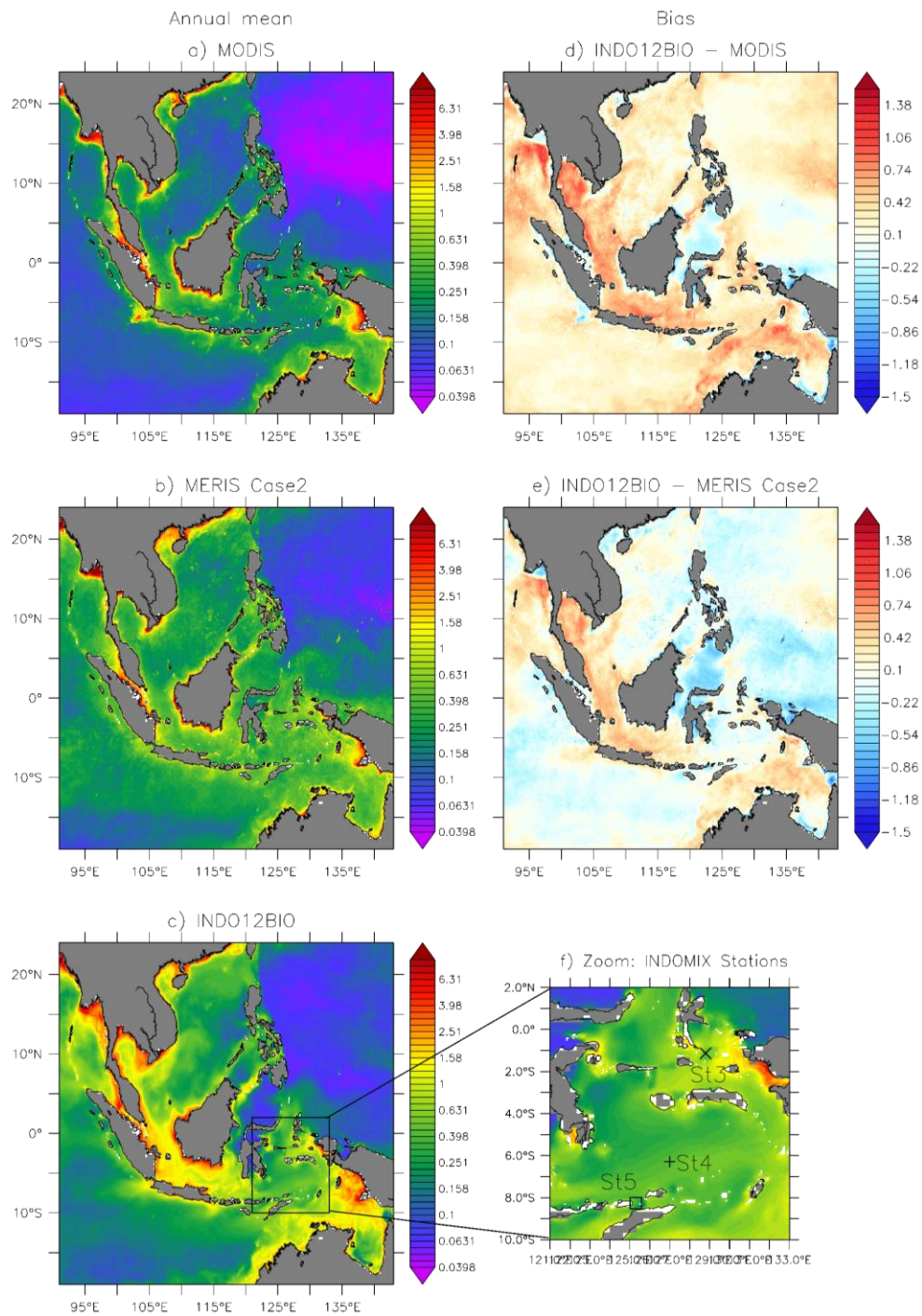


1

2 Figure 2: Annual mean of nitrate (mmol N m^{-3} ; left) and oxygen concentrations ($\text{ml O}_2 \text{l}^{-1}$;
 3 right) at 100 m depth from CARS (a, d) and WOA (b, e; statistical mean) annual
 4 climatologies, and from INDO12BIO as 2010-2014 averages (c, f). Three key boxes for water
 5 mass transformation (North Pacific, Banda, and Timor; Koch-Larrouy et al., 2007) were
 6 added to the bottom-right figure.

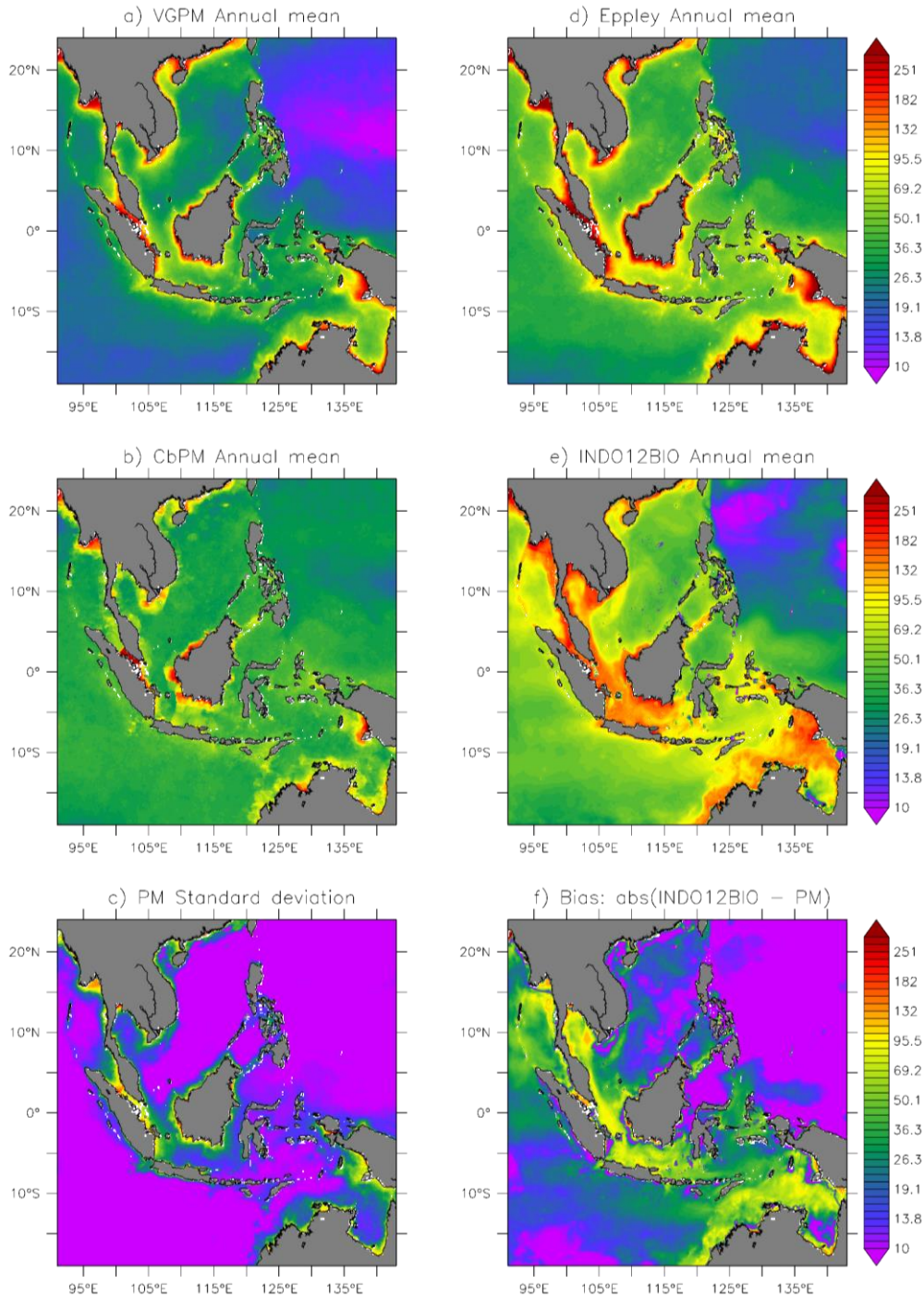


1
 2 Figure 3: Vertical profiles of oxygen ($\text{ml O}_2 \text{ l}^{-1}$; top: a, d, g), nitrate (mmol N m^{-3} ; middle: b,
 3 e, h) and dissolved silica (mmol Si m^{-3} ; bottom: c, f, i) in 3 key boxes for water masses
 4 transformation (North Pacific, left; Banda, middle; and Timor, right) (see Fig. 2; Koch-
 5 Larrouy et al., 2007). CARS and WOA annual climatologies are in red and dark blue.
 6 INDO12BIO simulation averaged between 2010 and 2014 is in black. All the raw data
 7 available on each box and gathered in the WOD (light blue crosses) are added in order to
 8 illustrate the spread of data.



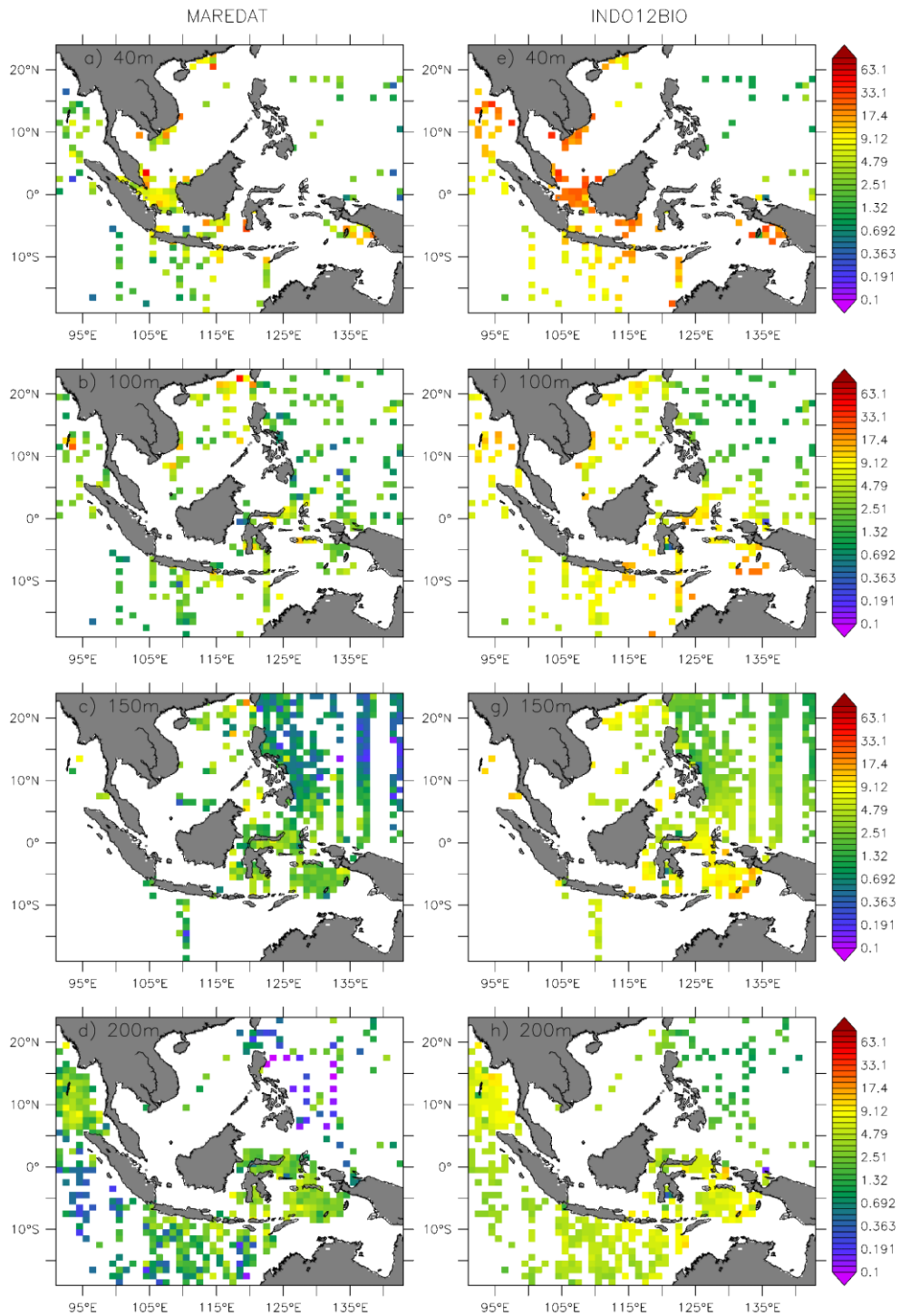
1

2 Figure 4. Left) Annual mean of surface chlorophyll-*a* concentrations (mg Chl m⁻³) for year
 3 2011: MODIS Case-1 product (a), MERIS Case-2 product (b) and INDO12BIO simulation
 4 (c). Right) Bias of log-transformed surface chlorophyll (model-observation) for the same
 5 year. The model was masked as a function of the observation, MODIS Case-1 (d) or MERIS
 6 Case-2 (e). Location of 3 stations sampled during the INDOMIX cruise and used for
 7 evaluation of the model in Section 4.4 (f).



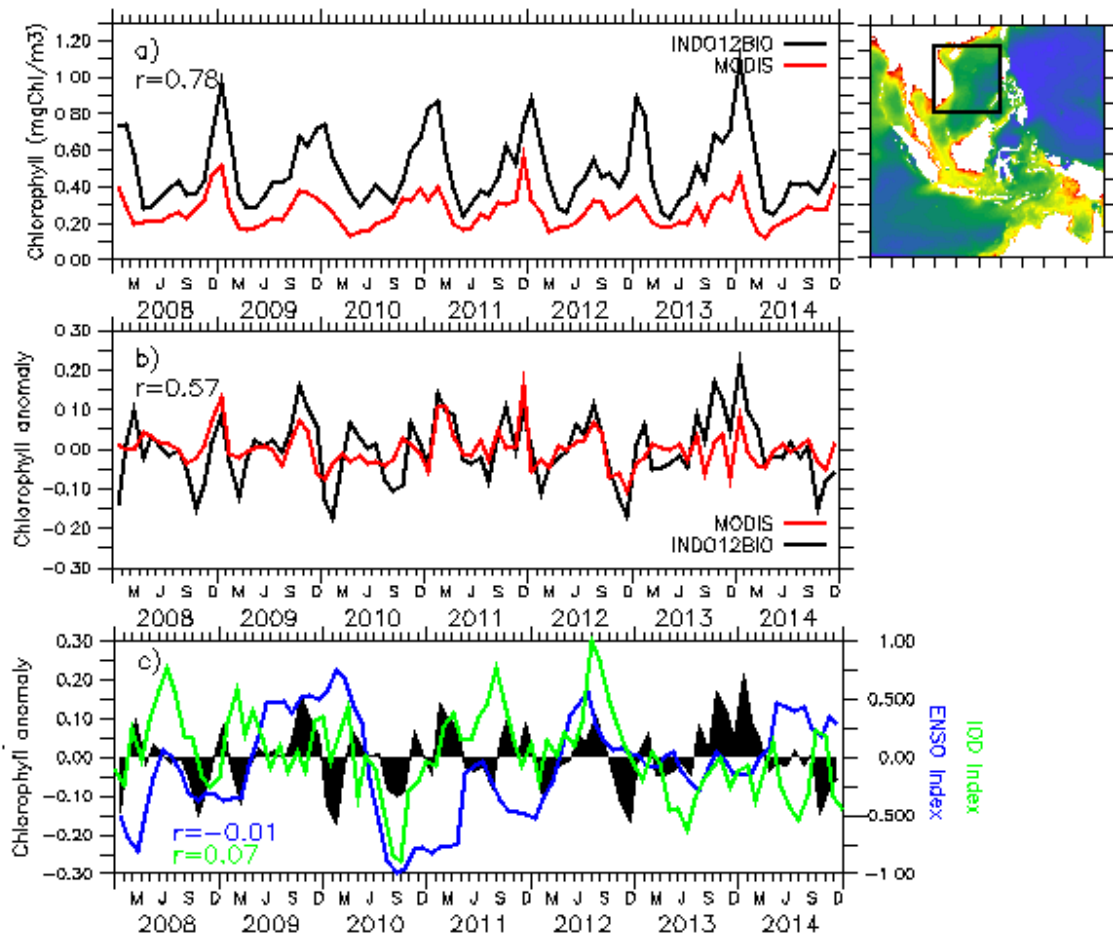
2

3 Figure 5. Annual mean of vertically integrated NPP ($\text{mmol C m}^{-2} \text{d}^{-1}$) for year 2011: VGPM
 4 (a), Eppley (d), and CbPM (b) production models, all based on MODIS ocean colour, as well
 5 as for INDO12BIO (e). Standard deviation of the 3 averaged production models (PM) (c), and
 6 bias between INDO12BIO and the averaged PM (f).

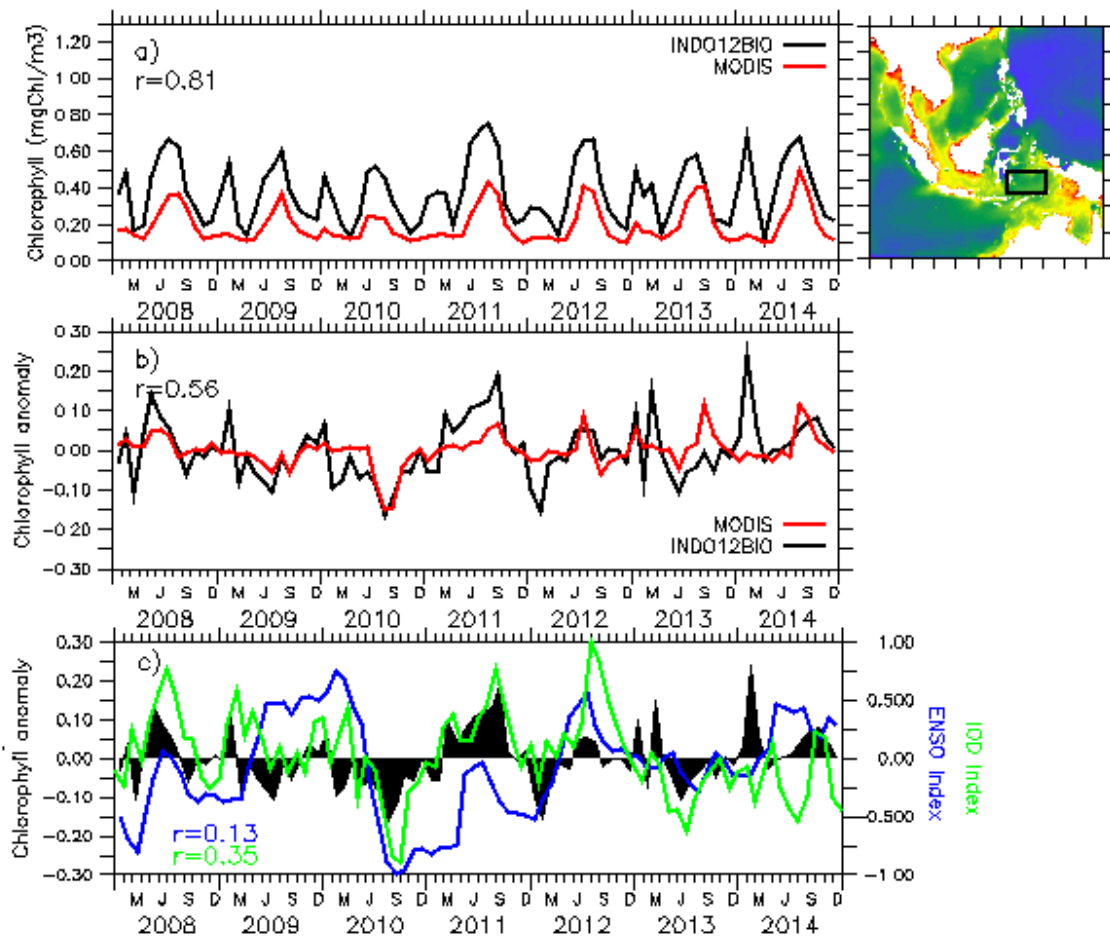


1

2 Figure 6: Annual mean of mesozooplankton biomass ($\mu\text{g C l}^{-1}$) from MAREDAT monthly
 3 climatology (left) and from INDO12BIO simulation averaged between 2010 and 2014 (right),
 4 for distinct depth interval: from the surface up to 40m (a, e), 100m (b, f), 150m (c, g), and
 5 200m depth (d, h). Simulated fields were interpolated onto the MAREDAT grid, and masked
 6 as a function of the data (in space and time).

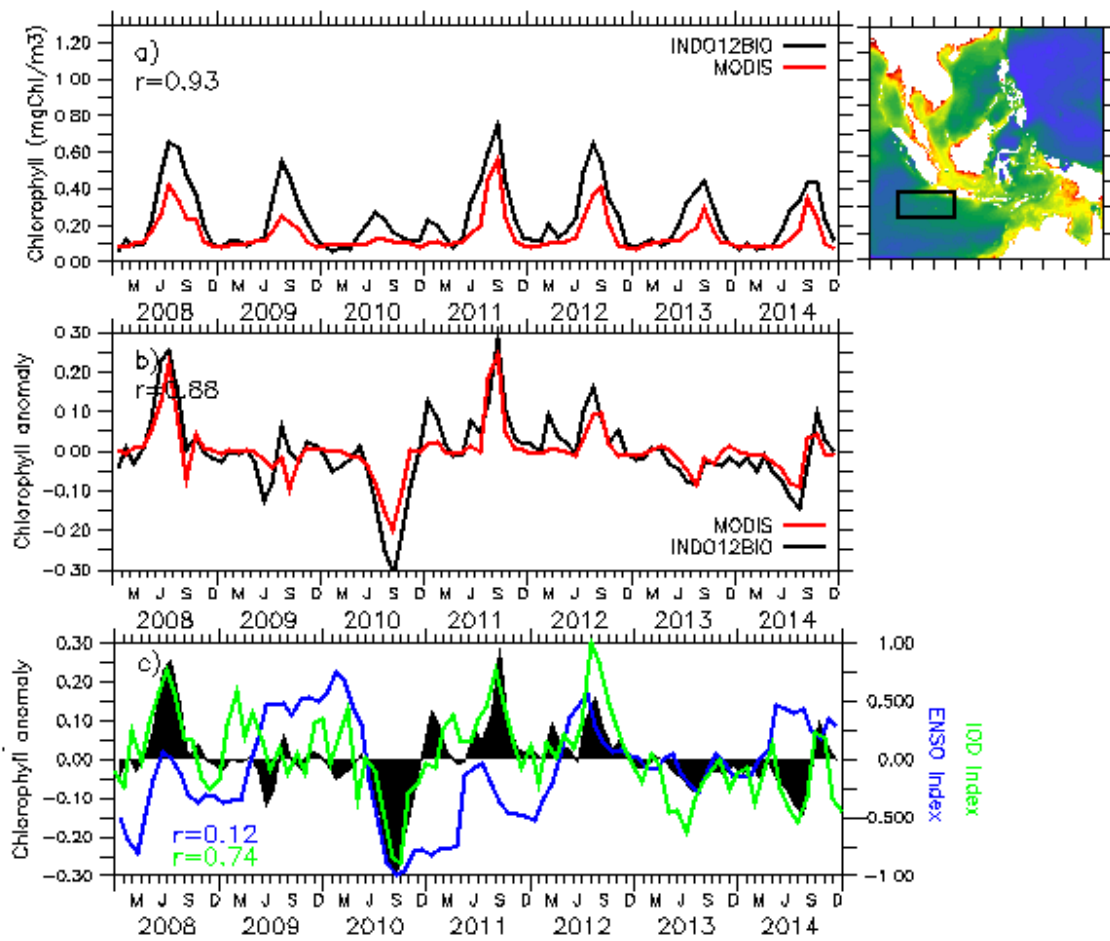


1
 2 Figure 7: a) Mean surface chlorophyll-*a* concentrations and b) its interannual anomalies (mg
 3 Chl m⁻³) over the South China Sea. INDO12BIO is in black and MODIS Case-1 in red.
 4 Temporal correlation (*r*) between both time series is in black. c) ENSO (blue) and IOD
 5 (green) phenomena are respectively represented by MEI and DMI indexes. Indexes were
 6 normalized by their maximum value in order to be plotted on the same axis. Interannual
 7 anomalies of simulated chlorophyll-*a* reminded in black. Temporal correlation (*r*) between the
 8 simulated chlorophyll-*a* and ENSO (IOD) is indicated in blue (green).



1

2 Figure 8: Same as Figure 7, in Banda Sea.

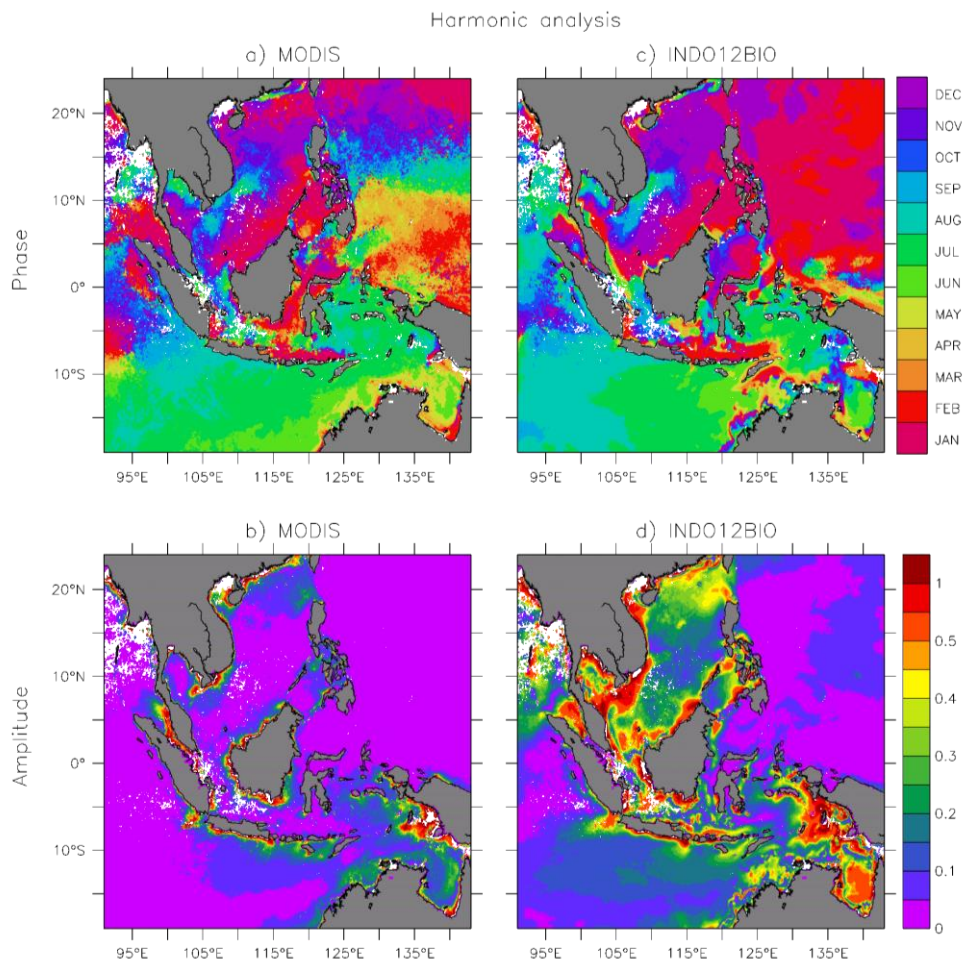


1

2 Figure 9: Same as Figure 7, in Sunda area.

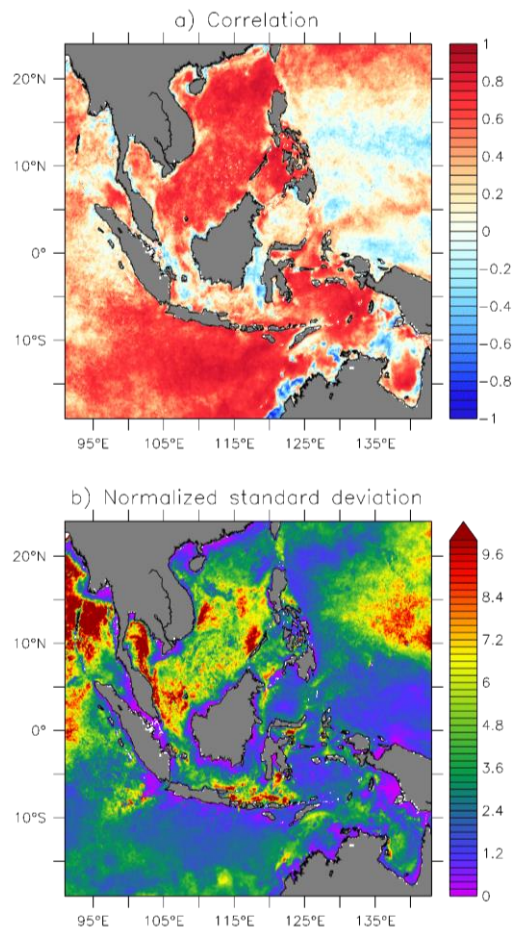
3

4



1

2 Figure 10. Timing of maximum chlorophyll-*a* (a, c) and amplitude (b, d) for a monthly
 3 climatology of surface chlorophyll-*a* concentrations between 2010 and 2014: MODIS Case-1
 4 (left) and INDO12BIO (right). The model was masked as a function of the data.

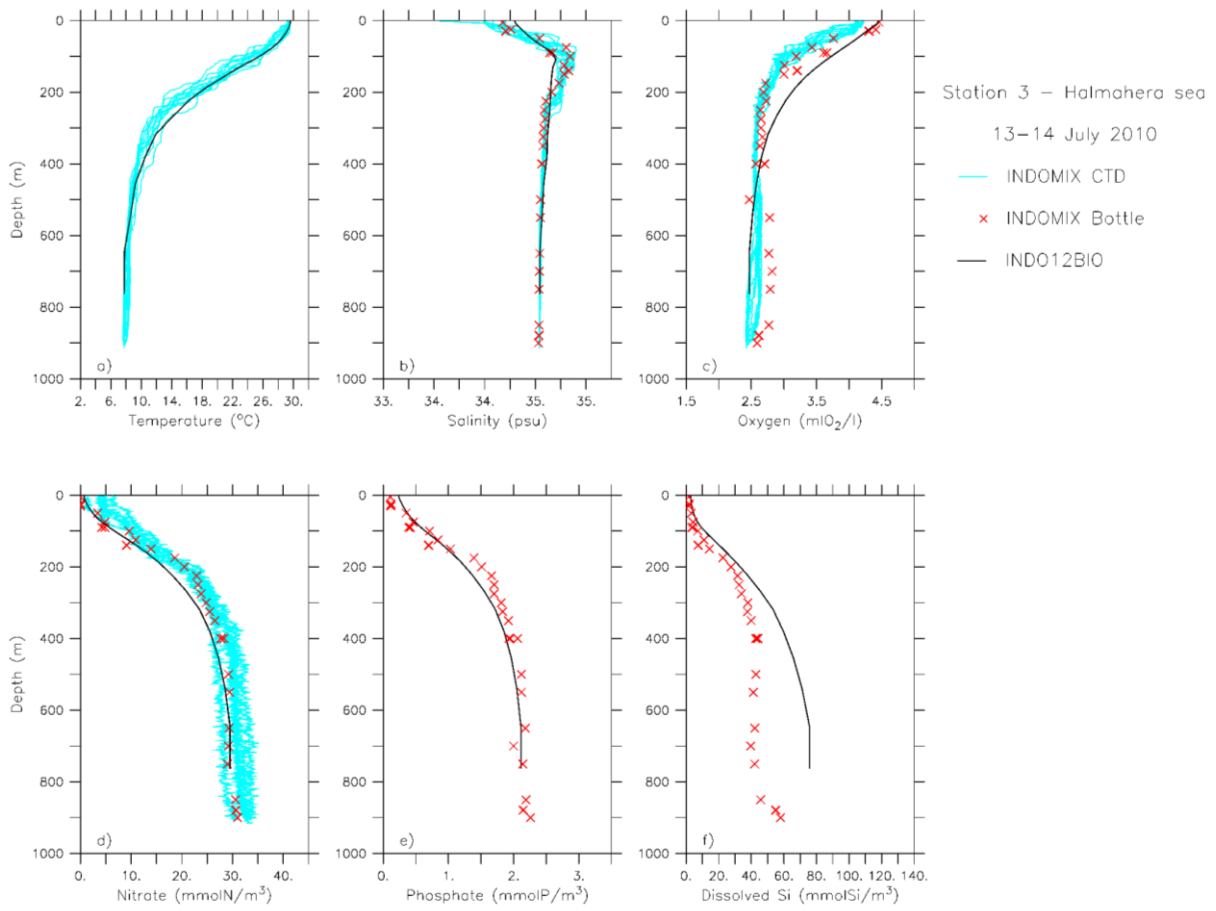


1

2 Figure 11: Temporal correlation (a) and normalised standard deviation (b;
 3 $\text{std}(\text{model})/\text{std}(\text{data})$) estimated between the INDO12BIO simulation and the MODIS Case-1
 4 ocean colour product. Statistics are computed on monthly fields between 2010 and 2014. The
 5 model was masked as a function of the data.

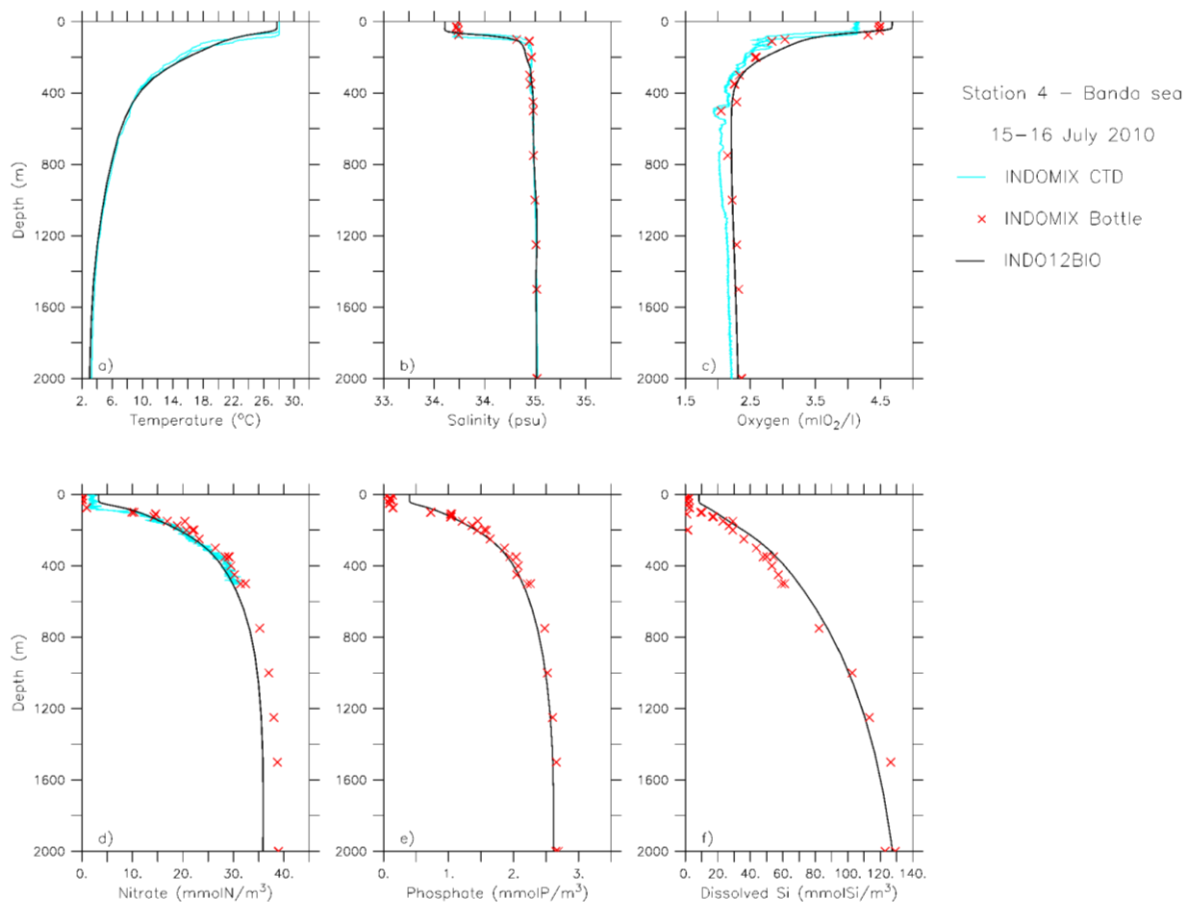
6

1

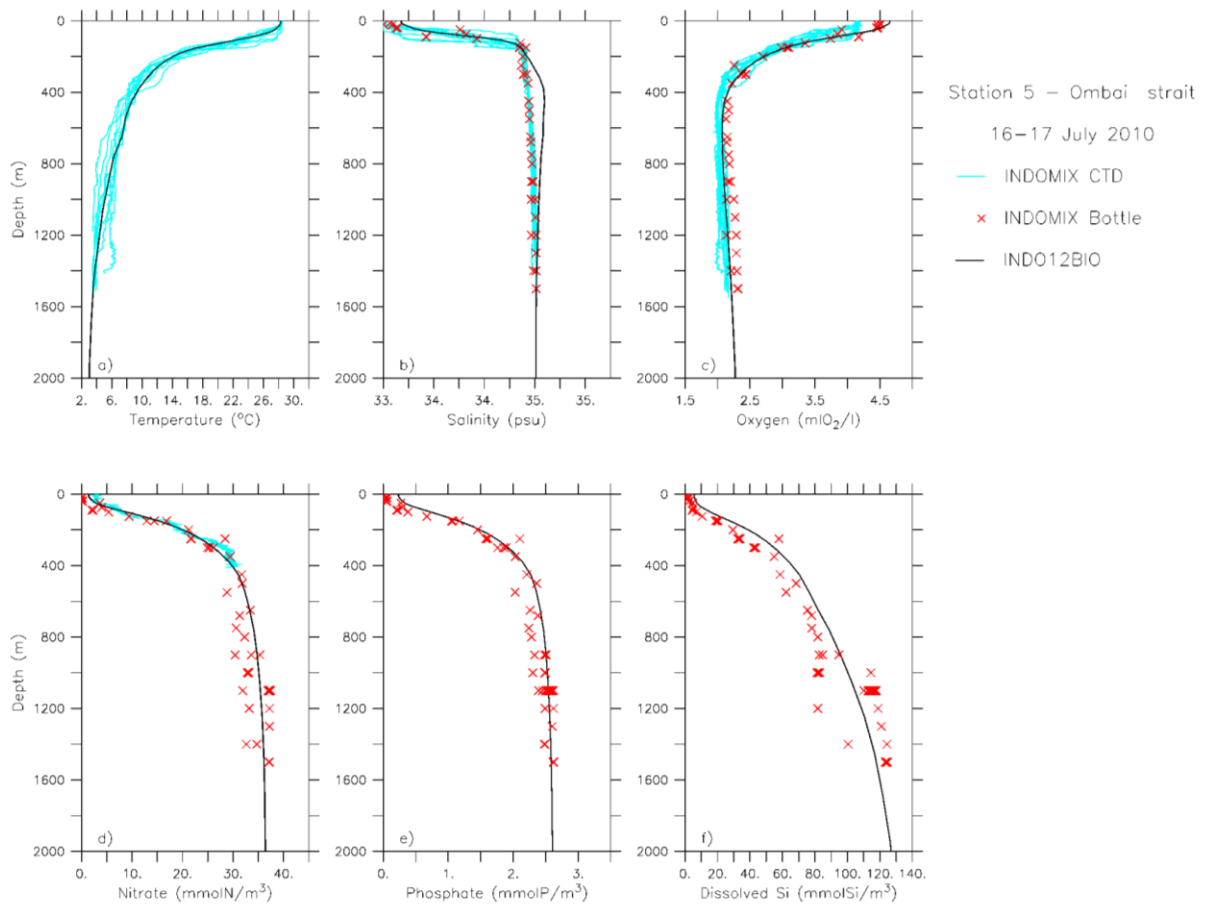


2

3 Figure 12: Vertical profiles of temperature ($^{\circ}\text{C}$; a), salinity (psu; b), oxygen ($\text{ml O}_2 \text{ l}^{-1}$; c),
4 nitrate (mmol N m^{-3} ; d), phosphate (mmol P m^{-3} ; e), and dissolved silica (mmol Si m^{-3} ; f)
5 concentrations at INDOMIX cruise Station 3 (Halmahera Sea; 13 - 14 July 2010). CTDO or
6 ISUS sensor (light blue lines) and bottle (red crosses) measurements represent the conditions
7 during cruise, 2-day model averages are shown by the black line.



1
2 Figure 13: Vertical profiles of temperature ($^{\circ}\text{C}$; a), salinity (psu; b), oxygen ($\text{ml O}_2 \text{ l}^{-1}$; c),
3 nitrate (mmol N m^{-3} ; d), phosphate (mmol P m^{-3} ; e), and dissolved silica (mmol Si m^{-3} ; f)
4 concentrations at INDOMIX cruise Station 4 (Banda Sea; 15 - 16 July 2010). CTDO or ISUS
5 sensor (light blue lines) and bottle (red crosses) measurements represent the conditions during
6 cruise, 2-day model averages are shown by the black line.



1
2 Figure 14: Vertical profiles of temperature ($^{\circ}\text{C}$; a), salinity (psu; b), oxygen ($\text{ml O}_2 \text{ l}^{-1}$; c),
3 nitrate (mmol N m^{-3} ; d), phosphate (mmol P m^{-3} ; e), and dissolved silica (mmol Si m^{-3} ; f)
4 concentrations at INDOMIX cruise Station 5 (Ombai Strait; 16 - 17 July 2010). CTDO or
5 ISUS sensor (light blue lines) and bottle (red crosses) measurements represent the conditions
6 during cruise, 2-day model averages are shown by the black line.

7